International Journal of Disaster Risk Reduction 133 (2026) 106003

Contents lists available at ScienceDirect

International Journal of Disaster Risk Reduction

journal homepage: www.elsevier.com/locate/ijdrr

# Enhancing the resilience of wind energy infrastructure in Iowa: Flood risk assessment and site suitability analysis for critical infrastructure protection

Ege Duran [a,b,*], Ibrahim Demir [c,d]

[a] IIHR Hydroscience and Engineering, University of Iowa, Iowa City, IA, USA
[b] Civil and Environmental Engineering, University of Iowa, Iowa City, IA, USA
[c] River-Coastal Science and Engineering, Tulane University, New Orleans, LA, USA
[d] ByWater Institute, Tulane University, New Orleans, LA, USA

ARTICLE INFO

*Keywords:*
Flood impact
Wind turbine
Zonal statistics
Disaster risk assessment
Critical infrastructure

ABSTRACT

As climate change increases the frequency and severity of hydrological hazards, understanding and reducing disaster risk to renewable energy infrastructure has become critical. Iowa, a national leader in wind energy generation, faces enhanced vulnerability due to the intersection of extensive wind turbine deployment and increasing flood risk. This study provides a comprehensive geospatial and statistical evaluation of flood exposure and site suitability for future installation of wind turbines across Iowa, using zonal statistics within buffer areas to evaluate spatial variation in elevation, soil drainage, flood depth, and mean wind profile. Correlation analysis reveals that turbine vulnerability is strongly linked to topographic variability ($r \approx 0.98$), and soil characteristics ($r \approx 0.79$), underscoring terrain as a key control on localized flood severity. Statewide results show that turbine exposure increases with spatial extent, from about 4 % near turbine bases to over 60 % at broader surroundings, underscoring the sensitivity of flood risk to buffer expansion and indicating that current siting practices may not sufficiently mitigate flood hazards. The research proposes targeted, data-driven recommendations for enhancing the resilience and continuity of wind generation as a vital component of the state's energy infrastructure. These insights support policymakers, engineers, and stakeholders in devising proactive flood mitigation strategies, reinforcing the reliability and security of Iowa's critical energy sector against evolving climate threats.

## 1. Introduction

Climate-related emergencies have become more frequent and severe in recent years, highlighting the critical need to address their consequences [1]. In particular, floods are among the most devastating natural disasters worldwide, and their impact is worsened by climate change, population growth, and rapid urbanization [2,3]. As a result, they have become a major global risk, causing substantial economic losses, displacement, and damage to infrastructure [4–6], with long-term consequences for ecosystems and communities [7]. Flood disasters can be triggered by rainfall patterns, severity, and distribution, as well as land cover, soil moisture, and stream-network capacity [8,9]. The unpredictability of floods, characterized by sudden onset, durations from days to weeks depending on terrain and

* Corresponding author. IIHR Hydroscience and Engineering, University of Iowa, Iowa City, IA, USA.
*E-mail address:* ege-duran@uiowa.edu (E. Duran).

https://doi.org/10.1016/j.ijdrr.2026.106003
Received 14 July 2025; Received in revised form 16 December 2025; Accepted 8 January 2026
Available online 9 January 2026

drainage, magnifies recovery challenges [10]. Within this context, it is important to examine how variations in elevation and soil drainage capacity influence the susceptibility of wind turbines to floods in Iowa, where the escalating frequency and severity of flooding events heighten infrastructure risk [11].

As fossil fuel reserves such as coal, oil, and gas become scarcer and environmental concerns grow, the global economy's expansion and rising energy consumption make it urgent to find reliable renewable alternatives [12–14]. Wind energy has become a major solution due to its availability and cost-effectiveness, reshaping electricity generation [15],16,17 and playing a pivotal role in energy sustainability [18]. Iowa presents a critical case study given its heavy reliance on wind power and abundant wind resources. As a national leader in renewable energy, the state hosts 6345 wind turbines that supply nearly two-thirds of its electricity [19,20]. Most turbines are concentrated in northwest and north-central Iowa, where wind conditions are ideal [21]. The state's landscape, bounded by the Mississippi River to the east and the Missouri River to the west, concentrates flood exposure, and historic events, especially in 2008, demonstrate its vulnerability [22–26]. Wind turbines may be situated at higher elevations yet remain susceptible to inundation and access disruption, underscoring the need for thorough flood-impact assessment to preserve energy-system stability.

Flood-risk assessment for infrastructure systems has been guided by several frameworks that emphasize hierarchical relationships among hazard, exposure, vulnerability, and resilience components [27]. Similarly, Peck et al. [28] introduced the Flood Adaptation Hierarchy, which provides a structured pathway for infrastructure adaptation by prioritizing avoidance, resistance, and recovery strategies. Iowa-focused flood work has advanced mitigation and risk assessment for transportation networks [29], public transit systems [30], critical amenities ([31]), properties [32], urban communities [33], and agricultural areas [34]. However, flood-risk evaluation for energy infrastructure, particularly wind turbines, remains largely unexplored.

Wind turbine related studies analyze flood profiles [35], drainage capacity [36], and soil characteristics [37] as separate drivers, while broader energy-system models consider grid planning and integration of wind into transmission networks [38]. Moreover, several studies have employed multi-criteria decision-making (MCDM) frameworks to evaluate wind energy site suitability, integrating diverse environmental, technical, and socioeconomic factors through weighted scoring systems [39]. In Iowa case, there are several feasibility studies with economical and wind performance-based analyses [15,40,41], yet none of these studies have integrated flood risk assessments into wind energy infrastructure planning, making this study a crucial step in bridging this gap by addressing the vulnerabilities of wind turbines to flooding.

Our analytical approach employs geospatial and statistical tools, including buffer-based zonal statistics and correlation analysis, to examine relationships among elevation variability, flood risk, and wind turbine vulnerability. Buffer zone analysis is a commonly used method in flood-related studies [42]. In this study, it is applied from a critical-infrastructure perspective, with wind turbines serving as the central spatial reference. This perspective aligns with recent infrastructure-based buffer assessments that prioritize asset-specific exposure analysis to improve hazard mitigation [43]. While MCDM methods are effective for general ranking, such approaches inherently depend on expert judgment to assign hierarchies among the parameters, introducing potential subjectivity and inconsistency across studies. In contrast, our study adopts a filtering-based framework that relies on direct elimination through predefined quantitative thresholds for flood exposure and wind profile suitability. This approach eliminates the need for subjective weighting or hierarchical structuring, thereby enhancing objectivity and transparency, as all decision rules are explicitly stated and reproducible. Moreover, it strengthens methodological consistency, since identical datasets and parameters will always yield the same outcomes. Despite this simplification, the filtering process remains fully compatible with conventional siting criteria and can be readily integrated into broader decision-support or regulatory evaluation workflows.

By translating our analysis into practical solutions that safeguard Iowa's renewable energy infrastructure against flooding, this study advances both community resilience and scientific understanding. We evaluated the possible effects of flooding on Iowa's energy supply, paying particular attention to risks posed by flood events that occur once every 100 and 500 years. Using vacant-land data, flood maps, and multi-annual average statewide wind profiles, we identified suitable locations for future turbine installations defined by optimal wind conditions and low flood exposure. While wind turbine developers already consider factors such as wind resources, land constraints, and grid access, our work introduces a dedicated flood-risk layer that complements existing decision frameworks of the opportunities and challenges for wind infrastructure in flood-prone regions. These findings provide a practical basis for policymakers to prioritize resilient energy-infrastructure investments and refine zoning practices in flood-prone regions, while guiding energy planners in balancing generation efficiency with long-term hazard mitigation. Collectively, the outcomes strengthen the link between renewable-energy expansion and climate-adaptation policy in Iowa, supporting a more reliable and sustainable energy landscape.

The remainder of this study is structured into methodology, results and discussion, and conclusion. The methodology details data preparation, buffer-based zonal statistics, correlation analysis, capacity-impact assessment, and site screening; the results and discussion present findings and implications; and the conclusion summarizes broader relevance for resilient wind-energy planning in flood-prone regions.

## 2. Methodology

This section outlines the process utilized to assess how flooding affects wind turbines and identify potential sites for new installations. In order to evaluate the existing turbines' flood vulnerability, the process starts by defining buffer zones around them. After that, elevation, drainage capacity, and flood depth within these zones are examined. Calculating key metrics like average elevation and its variance aids in understanding how terrain affects turbine risk. The relationships between elevation, flood risk, and turbine vulnerability are investigated through correlation analysis, which identifies the best locations for new turbines based on factors like wind efficiency and flood safety.

### 2.1. Data preparation

This study incorporated multiple geospatial datasets to evaluate flood exposure and wind turbine suitability in Iowa. Existing turbine locations were obtained from the United States Geological Survey (USGS) U.S. Wind Turbine Database [44], which provides coordinate-based turbine inventories. Elevation data were derived from the Iowa Department of Natural Resources [45] digital elevation model, available at 30m resolution, suitable for fine-scale terrain analysis. Flood hazard conditions were represented using the Iowa Statewide Floodplain Mapping Project (geodata.iowa.gov, 2023), which provides 100-year and 500-year return period flood scenarios modeled with HEC-RAS and MIKEFLOOD. These data are distributed as 1m raster tiles organized by HUC-8 watersheds, supporting detailed inundation assessment around turbine sites. Soil conditions were characterized by the Iowa Soil Drainage Class maps (gSSURGO-based, 10m resolution) from the Iowa State University GIS Facility [46]. These datasets classify soils by drainage capacity and were later normalized into ordinal scores for statistical correlation with turbine areas. Wind resource data were incorporated from the National Renewable Energy Laboratory (NREL) Wind Integration National Dataset (WIND) Toolkit [47–50]. The dataset provides modeled multi-year annual average wind speeds at 80 m and 100 m hub heights for the period 2007–2013, at a 2 km × 2 km resolution. The raster datasets were clipped to the Iowa boundary and integrated without resampling, as the multi-year averaging ensures robustness and resizing could introduce distortions. Base reference layers were obtained from OpenStreetMap [51] and used for visualization and contextual mapping.

All datasets were projected into a consistent coordinate system, clipped to the state boundary, and processed for use in zonal statistics and correlation analyses. Table 1 summarizes the datasets with their resolution and source, while Fig. 1 presents a visualization of the primary geospatial layers. Together, the tabular and visual representations enhance transparency and reproducibility, providing a clear foundation for the subsequent methodological steps.

### 2.2. Zonal analysis with buffer extensions

This section presents the reasoning behind the steps taken in preparing and analyzing the data, as well as the tools used for each phase. Our initial step involved importing each data set into a GIS software tool and reproducing them to ensure uniformity in coordinate systems across all layers. Following this, we created base buffer zones for each wind turbine location. Wind turbines are generally constructed with foundations 15–25 m wide, depending on the structure, which are roughly 4 to 5 times larger than the turbine body. In addition, there has been a recent trend toward the construction of taller wind turbines, which increases the probability of damage in the case of a superstructure failure, as the taller structures require larger foundations [52]. When placing a turbine, it is important to consider soil texture and stress distribution, represented by the pressure bulb beneath the wind turbine foundation and associated foundation construction details illustrated in Fig. 2, to ensure foundation stability [53]. Moreover, the horizontal area impacted by stress distribution can rise 2 to 2.5 times the foundation size influenced by factors like structure weight, foundation size, and soil type, as stated by wind turbine corporations like CNBM International Wind Power [54].

During the lifespan of a wind turbine, the foundation is exposed to not only static loads but also dynamic forces, including fluctuating wind pressures and moment-induced stresses, which cause variations in the stress distribution beneath the foundation. These factors necessitate intricate foundation designs, particularly for taller turbines that require larger, more stable foundations [55]. To ensure a cautious and standardized approach, a 100m buffer zone was selected as the base for flood risk analysis. While stress distribution extends beyond the foundation footprint, the interaction between flood-induced soil saturation and foundation integrity remains complex due to variations in soil type, turbine design, and hydrological conditions. This buffer distance provides a conservative estimate of the directly impacted zone, encompassing the primary area where floodwater infiltration could alter soil mechanical properties and affect turbine stability. Moreover, given the variation in turbine foundations across Iowa state, this approach ensures methodological consistency while allowing for a progressive analysis of flood impact from 100m to 1,000m in 50m increments. This systematic framework enables an adaptable assessment while maintaining feasibility within the scope of this study.

To fully capture the range of elevation changes and flood depths around each wind turbine, we used circular buffer shapes instead of the traditional square or rectangular ones. The circular shape lets us include elevation data from all directions around the wind turbine, which gives us a more complete picture of the terrain. By using circular buffers, we consider the spatial variations in terrain

**Table 1**
Description of datasets used in this study, indicating their role in the analysis, spatial resolution, and source.

| Dataset | Purpose in Study | Resolution/Format | Source |
|---|---|---|---|
| Wind Turbine Locations | Identify existing turbine sites, their capacities, buffer creation, and flood exposure analysis | Point data (coordinates) | USGS – U.S. Wind Turbine Database (USWTDB) (2024) |
| Digital Elevation Model (DEM) | Elevation analysis, terrain variance, correlation with flood exposure | 30m raster (1 arc-second) | Iowa DNR Elevation Dataset (2022) |
| Flood Depth and Extent | Define flood risk zones, inundation statistics, capacity exposure assessment | 1m raster (.jp2, HUC-8 tiles) | Iowa Statewide Floodplain Mapping Project (HEC-RAS & MIKEFLOOD, geodata.iowa.gov) (2023) |
| Soil Drainage Class Map | Assess land suitability, normalize drainage scores, correlate with turbine areas | 10m raster (gSSURGO-based) | Iowa State University GIS Facility [46] |
| Wind Resource Data (80m & 100m hub height) | Evaluate site suitability for new turbine placement based on annual mean wind speeds | 2 km × 2 km raster | National Renewable Energy Laboratory (NREL WIND Toolkit) (2015) |
| Base Maps | Visualization and contextual analysis | Vector/Raster | OpenStreetMap [51] |

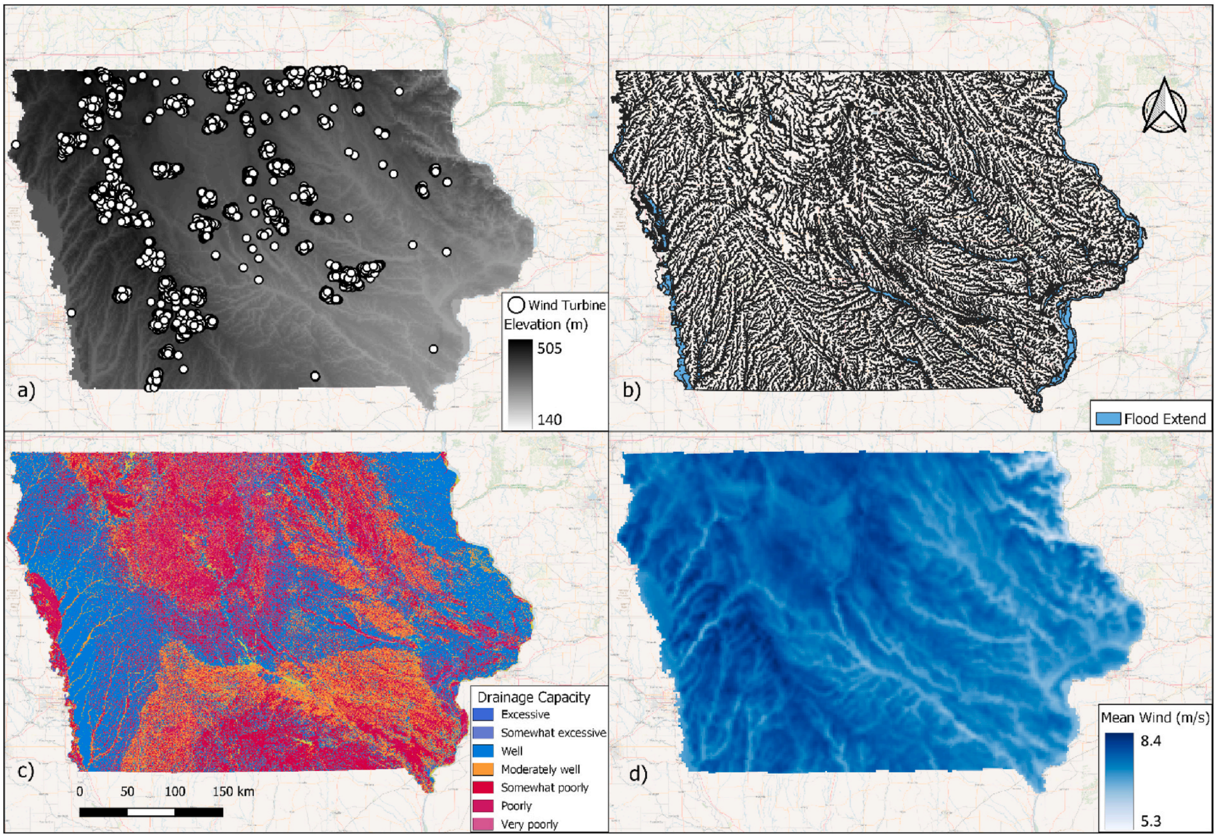


**Fig. 1.** Iowa State database representation: a) wind turbine locations overlaid with the mean elevation profile of Iowa; b) 500-year flood extent map; c) distribution map of drainage capacity; d) annual mean wind profile at 100-m height.

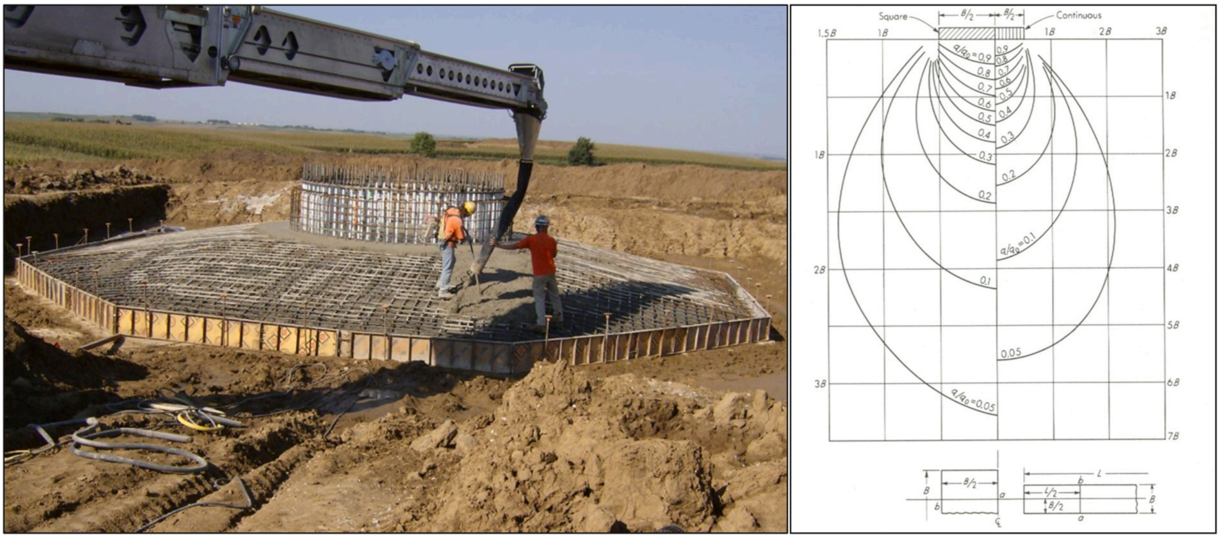


**Fig. 2.** Sample foundation of wind turbine (Ashlock & Schaefer, 2011) and stress distribution isobars of that (GEO-SLOPE International Ltd, 2024).

features, ensuring that we consider elevation and flood data from every angle in our analysis.

As illustrated in Fig. 3, we expanded the buffer zones for wind turbines at various distances (e.g., 100m, 150m, up to 1,000m) using GIS software. While commonly used extension distances like 100m, 500m, and 1,000m are referenced in flood risk assessments with a critical infrastructure–centered perspective (e.g., [56]); to capture spatial trends more precisely, we increase the buffer size in 50m intervals and carry out detailed zonal statistical and correlation analyses. In related environmental and hazard-based analyses, Fang et al. [57] applied multi-ring buffers around linear hazard factors (e.g., roads and rivers) in landslide-susceptibility mapping and showed that hazard correlation strength changes with buffer distance, emphasizing the need to evaluate multiple radii. Similarly, Pervez et al. [58] developed a multi-scale land-use regression model in which predictor variables were computed across several buffer sizes (25–1,000m) to reveal how exposure influence decays with distance. Drawing from these approaches, our incremental design produced realistic, spatially coherent results—the elevation and flood-susceptibility gradients exhibited no artificial fragmentation across radii, confirming that the 50 m steps preserve topographic continuity while enabling a finer statistical resolution for correlation analysis and graphical visualization. It is also essential that these buffer zones remain accessible during flood events to ensure smooth maintenance and repairs. By concentrating on areas with significant elevation changes, particularly those that shift from flat to sloped terrain, this research tackles the important issue of accessibility during floods. Examining the connection between elevation variance and flood risk provides valuable insights into how different terrain features impact wind turbine susceptibility. As anticipated, turbines in regions with notable elevation changes encounter greater challenges during floods, due to the higher likelihood of inundation in these areas. Understanding these dynamics is key to developing effective strategies to enhance the resilience of wind energy infrastructure in flood-prone areas.

Fig. 3 shows the locations of wind turbines with their corresponding 100m, 500m, and 1,000m buffer zone expansions. The inset zooms into a specific area, highlighting three wind turbines and their buffer zones. These zones are appropriately scaled to avoid exaggerating flood impact values and are designed to analyze how flood impact varies with distance from the turbine foundations. Unlike riparian assessments, which typically expand water body buffers to analyze spatial impacts, our study focuses not only on flood extent but also on flood depth. Since flood depth varies within the floodplain, we expand the buffer zones around wind turbines rather than the flood extent buffers to avoid overestimating flood depth values. Incremental buffer expansions help capture spatial trends, and the observed strong correlation across zones. The overlay of flood extent and elevation in Fig. 3 further demonstrates that only a portion of turbine buffer zones intersect with mapped flood-prone areas. While the flood extents most frequently intersect the 1,000m buffer zones, they also extend into the 500m and 100m zones, underscoring the importance of considering all buffer zones in flood risk assessments. Even the smallest zones can be affected, with implications for the safety and long-term planning of wind turbine sites.

While wind turbines are generally resilient to flooding due to their elevated design, we assume that if a turbine is located within a flood zone, its operation could be compromised by both direct impacts, such as electrical infrastructure failures or foundation instability, and indirect consequences, such as restricted maintenance access and grid disruptions. Wind farms rely on a network of roads, transformers, and substations, so flood events in the surrounding area can still present significant operational challenges, even if the turbines themselves remain physically intact. In our assessment, we focused on the exposure of wind turbines to flood zones rather than applying a specific damage function, as no widely accepted depth-damage curve for wind turbines is available in the existing

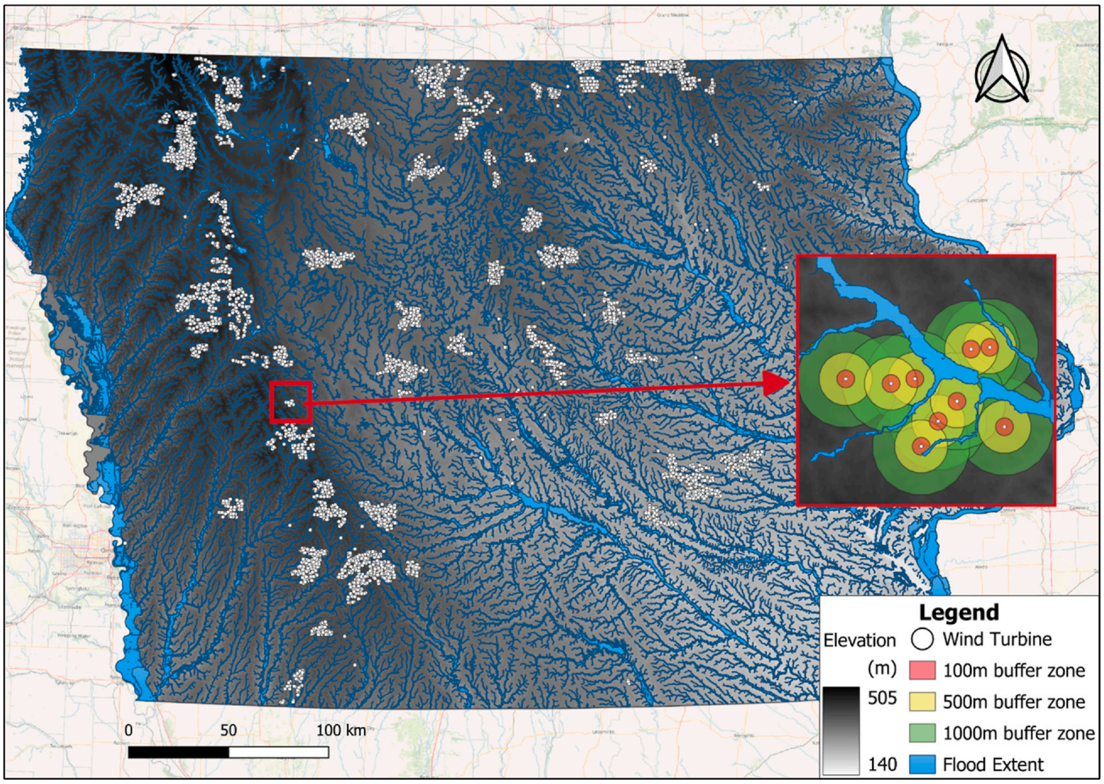


**Fig. 3.** Iowa wind turbine locations with defined buffer zones (100, 500, and 1,000m), overlaid with flood extent and elevation information.).

literature.

One of the contributing factors to floods and waterlogging is the inadequate infiltration ability and particularly insufficient drainage capacity of surface layers in the landscape (Deasy et al., 2014). In this section, we intersected our turbine locations with the main soil profile raster in Iowa obtained from the Iowa Soil Drainage Class [46], which are based on the classification system outlined in the USDA NRCS Soil Survey Manual [59]. The drainage classification, order, and normalized values are detailed in Table 2.

Since the original dataset provides qualitative drainage classifications rather than a numerical scoring system, we applied an ordinal ranking and normalization approach to maintain relative differences between classes while enabling quantitative correlation analysis. This normalization does not introduce bias into the results, as the correlation values depend on relative trends rather than absolute numerical assignments. For instance, excessively drained soils receive higher scores due to their rapid water drainage and minimal water retention capacity, whereas very poorly drained soils, which retain water excessively, are assigned lower scores, often resulting in prolonged waterlogging. This classification system aids in comprehending the suitability of soil for different purposes, such as agriculture, landscaping, or construction, by evaluating their drainage characteristics [60].

This scoring system was used specifically for correlation analysis to examine relationships between drainage ability and existing turbine areas, rather than as a direct input for capacity calculations or suitability assessment. The absolute numerical values assigned to each class do not influence the correlation trends since only the relative ranking of drainage conditions matters. Detailed explanations of this process are provided within the correlation calculations to ensure understanding.

### 2.2.1. *Zonal statistics*

Zonal statistics operate across both raster and vector data, in contrast to numerous geospatial methods that are limited to either raster or vector data exclusively [61]. Zonal statistics constitutes the cornerstone of this study, encompassing the computation of summary statistics (e.g., mean, range, variance) for raster data within predefined zones or regions. These zones are typically delineated by vector polygon features, such as administrative boundaries, study areas, or buffer zones surrounding specific features like wind turbines. The primary objective of zonal statistics is to furnish aggregated insights regarding raster datasets within each zone or region of interest. By deriving statistical summaries, zonal statistics empower researchers to analyze spatial patterns, discern trends, and evaluate relationships between raster data and spatial features.

Our study utilizes vector polygon features to define zones or regions of interest, as Fig. 4 illustrates. These zones here refer to the circular buffer zones that have been set up around the locations of the wind turbines. The use of circular buffers ensures that we capture the full range of spatial data surrounding each turbine. Once these zones are defined, we extract data from raster datasets such as elevation and flood depth within each zone. We can examine the spatial features of the regions surrounding the turbines thanks to this crucial step.

Once the necessary raster data is extracted, we proceed with calculating key statistical measures like the mean, median, and variance within each buffer zone. These statistics provide valuable insights into the variability and distribution of the data, allowing us to better understand the terrain and flood risks associated with the wind turbine locations. By analyzing this aggregated data, we can make well-founded conclusions about how spatial factors influence turbine placement and their susceptibility to environmental risks like flooding.

In the context of our research, statistical findings are essential for understanding the relationship between elevation variance, flood risk, and wind turbine vulnerability. We calculated key statistical parameters, including mean elevation, elevation range, variance, and standard deviation, to analyze terrain characteristics within buffer zones around each wind turbine. Mean elevation represents the average altitude within a buffer zone, while elevation range provides insight into topographic relief by measuring the difference between the highest and lowest elevation points. Variance and standard deviation quantify the spread and dispersion of elevation values, indicating the degree of terrain variability in each zone.

To assess flood vulnerability and delineate inundated buffer zones, we utilized flood-depth rasters for each flood scenario. Each scenario consisted of 55 raster layers corresponding to the HUC-8 watershed tiles that collectively cover Iowa. The layers were analyzed separately rather than mosaicked to a single surface to avoid introducing boundary artifacts or fractional mismatches along watershed borders. The analysis encompassed 6345 wind-turbine locations and 19 buffer-zone distances. Zonal-statistics tools were applied to extract the maximum flood-depth value within each turbine buffer from all intersecting tiles. Custom Python scripts developed with NumPy and Pandas automated this process by performing a row-wise maximum operation across overlapping datasets, retaining the deepest flood-depth value for each turbine–buffer pair. This rule provides a consistent and conservative measure of exposure, capturing the highest inundation potential in areas where multiple hydrologic units overlap, while maintaining uniform

**Table 2**
Drainage capacity classification and drainage score based on capacity order.

| Capacity Order | Drainage Capacity Classification | Ordinal Drainage Score |
|---|---|---|
| 1 | Excessively drained | 1.00 |
| 2 | Somewhat excessively drained | 0.83 |
| 3 | Well drained | 0.67 |
| 4 | Moderately well-drained | 0.50 |
| 5 | Somewhat poorly drained | 0.33 |
| 6 | Poorly drained | 0.17 |
| 7 | Very poorly drained | 0.00 |

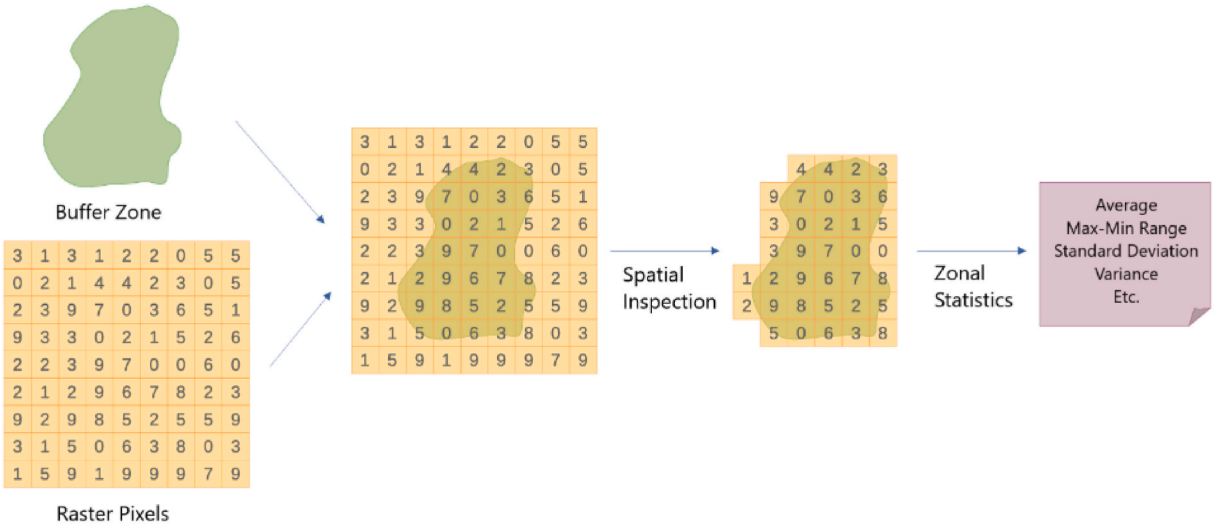


**Fig. 4.** Zonal statistic operation ([62], modified).

comparability across the statewide analysis.

In flood-risk research, exposure is commonly expressed through fractional inundation, depth-exceedance thresholds, or duration-based metrics [63–66]. These approaches are well suited to detailed, asset-specific analyses supported by hydraulic or structural data. In contrast, this study adopts a buffer-maximum-depth (buffer-max) method, designating a turbine's surrounding zone as exposed if any inundation occurs and using the maximum depth within that zone as the indicator of severity. This metric provides a consistent and conservative way to represent exposure across a large number of turbines and buffer radii, emphasizing the most critical inundation condition rather than spatially averaged or duration-weighted values. By aggregating this data, we aimed to develop a broad understanding of the terrain's dynamics, which is critical for informed decision-making.

### 2.2.2. *Correlation analysis*

Following this, we performed a correlation analysis to explore the relationships between elevation variance, flood risk, and wind turbine vulnerability. For each buffer radius (100–1000m, 50m increments), statewide averages of elevation variance, elevation standard deviation, mean elevation, and mean soil drainage were compared with flood depth and flooded zone counts. To aid with data representing the relationship among the variables, we use the Pearson correlation method. This method is suitable for normalized datasets, mostly with no outliers. The correlation process is demonstrated below in Equation (1), which describes how the Pearson coefficient (r) is calculated:

$$r = \frac{\sum (x_i - \overline{x})(y_i - \overline{y})}{\sqrt{\sum (x_i - \overline{x})^2 \sum (y_i - \overline{y})^2}} \qquad \text{Eq. 1}$$

In this equation, r is the Pearson correlation coefficient, $x_i$ and $y_i$ are individual values for two variables, and $\bar{x}$ and $\bar{y}$ are their respective mean values. The correlation coefficient can range between −1 and 1, with a positive value indicating a direct correlation and a negative value suggesting an inverse relationship. A Pearson correlation coefficient greater than 0.7 is generally considered a strong correlation [67].

To account for the limited number of observations, we computed 95 % confidence intervals (CI) using the Fisher's z-transformation [68,36]. For a sample of size n, the transformation is described in Equations (2) and (3):

$$z = \frac{1}{2} ln\left(\frac{1-r}{1+r}\right);\ SE = \frac{1}{\sqrt{n-3}} \qquad \text{Eq. 2, 3}$$

where $z$ is the Fisher-transformed correlation and $SE$ is the standard error. For the 95 % confidence interval, the lower and upper bounds of $z$ are computed as Equations (4) and (5):

$$z_{low} = z - 1.96{*}SE;\ z_{high} = z + 1.96{*}SE \qquad \text{Eq. 4, 5}$$

where 1.96 is the critical value of the standard normal distribution corresponding to a 95 % probability range. Finally, the bounds are back-transformed into correlation space by Equations (6) and (7):

$$r_{low} = \frac{e^{2(z_{low})} - 1}{e^{2(z_{low})} + 1};\ r_{high} = \frac{e^{2\left(z_{high}\right)} - 1}{e^{2\left(z_{high}\right)} + 1} \qquad \text{Eq. 6, 7}$$

By using this analysis, we were able to explore how elevation variance, flood risk, and the susceptibility of wind turbines interact. To strengthen the reliability of these results, confidence intervals were calculated for each correlation coefficient to reflect not only point estimates, but also their statistical uncertainty. This combined approach provides clear insights into the dynamics between these variables and reinforces the robustness of the findings, which can guide strategies to improve the resilience of wind energy infrastructure in regions vulnerable to flooding.

### 2.3. Inundation and capacity impact assessment

According to the wind turbine dataset, we can determine the installed capacities and assess the potential exposure of turbines under flood scenarios. As previously mentioned, Iowa relies heavily on wind energy [19], making it crucial to investigate these impacts. The turbine-rated capacity is the output power at the rated wind speed, provided by the manufacturer, ACP, or internet resources, measured in kilowatts (kW). A small subset of turbines lacked published capacity values and therefore could not be included in the capacity exposure assessment. In total, 61 turbines (0.95 % of Iowa's 6345-turbine inventory) were excluded. Table 3 summarizes the distribution of these excluded turbines across buffer zones and return periods. Although the specific capacity of these turbines is unknown, their number represents less than 1 % of the statewide inventory, indicating that their exclusion has negligible influence on the overall analysis.

To complement the inundation analysis, we also applied a bootstrap resampling approach to quantify uncertainty in the statewide exposure estimates. This procedure was carried out both at the individual turbine level and at the watershed level, allowing us to capture variability arising from statistical sampling as well as from spatial clustering of turbines. Confidence intervals were calculated using the same equations described in Section 2.2, ensuring consistency across analyses. This uncertainty assessment provides a reliable basis for interpreting statewide inundation exposure, and the resulting confidence intervals are presented in the Results section.

### 2.4. Future site determination

We carried out the location determination of potential wind-turbine placement with an emphasis on long-term flood safety. First, to get a suitable location, that area should be safe from future flood events for long-lasting feasibility. To ensure durable and resilient site selection, we adopted the 500-year (0.2 % annual-chance) flood scenario as the upper design constraint. This threshold aligns with FEMA's flood-risk management policy, which recommends that critical infrastructure and essential facilities be located outside the 500-year floodplain [69]. It represents a widely accepted benchmark for resilience-based planning and design in the United States. At the same time, this choice accounts for the non-stationary behavior of flood recurrence under changing climatic conditions. Since these flood periods are based on historic events, climate change and global warming can lead to an increase in the frequency of extreme flood events [70]. Consequently, an event currently classified as a 500-year flood may statistically occur more frequently in the future (e.g., comparable to a 200-year event). Accordingly, areas intersecting the spatial extent of the 500-year flood scenario were excluded from the analysis, and only locations outside this floodplain were retained as candidates for future wind-turbine siting.

Moreover, these locations should be efficient for wind speed to provide sufficient power generation capacity. According to the USGS wind turbine database, we have noted that over 82 % of wind turbines fall within the 80m–100m hub height range. To ensure consistency and optimize solutions, we've chosen wind profiles at both 80m and 100m levels as key filtering criteria. By using the GIS tool, we extract the wind profile for 80m and 100m and clip it into the Iowa State border. To define appropriate thresholds, we adopted a combined standards-based and statistical procedure anchored in the IEC 61400-1 turbine-class framework. The IEC standard specifies reference annual-mean hub-height speeds of 10.0, 8.5, 7.5, and 6.0 m/s for Classes I–IV [71]. Guided by these design values, we first applied 7.5 m/s at 80 m where the Class III reference for inland sites as our preliminary threshold. We then validated this value empirically by generating statewide histograms of annual-mean wind speed from the NREL WIND Toolkit, which confirmed that 7.5 m/s corresponds to the upper decile (>90 %) of Iowa's 80 m distribution. Since several national programs cite approximately 6.5 m/s (at 80 m) as a feasible lower limit for utility-scale deployment [72],73, we intentionally adopted the stricter Class III criteria to focus on high-efficiency, high-yield regimes. Applying the same percentile rule to the 100 m profile produced a threshold near 8.0 m/s, which aligns with the Class II–III boundary in IEC 61400-1. These consistent percentile-standard relationships ensure that both hub-height thresholds reflect internationally recognized turbine classifications while remaining regionally validated. To further test local stability, we incorporated $\pm$0.5 m/s sensitivity bands around each breakpoint (7.0–8.0 m/s at 80 m and 7.5–8.5 m/s at 100 m). Approximately 43.8 % of the 80 m dataset and 39.5 % of the 100 m dataset fall within these ranges, confirming that the chosen breakpoints lie within data-dense, statistically robust portions of each distribution.

Physically, these thresholds correspond to a meaningful transition in energy yield governed by the standard wind-power relation in

**Table 3**
Number of turbines excluded from capacity impact analysis due to missing capacity data.

| Flood Scenario | 100-year | | 500-year | |
|---|---|---|---|---|
| Zone | **Excluded (#)** | **% of Inventory** | **Excluded (#)** | **% of Inventory** |
| 100m | 5 | 0.08 | 5 | 0.08 |
| 500m | 22 | 0.35 | 23 | 0.36 |
| 1,000m | 45 | 0.71 | 48 | 0.76 |

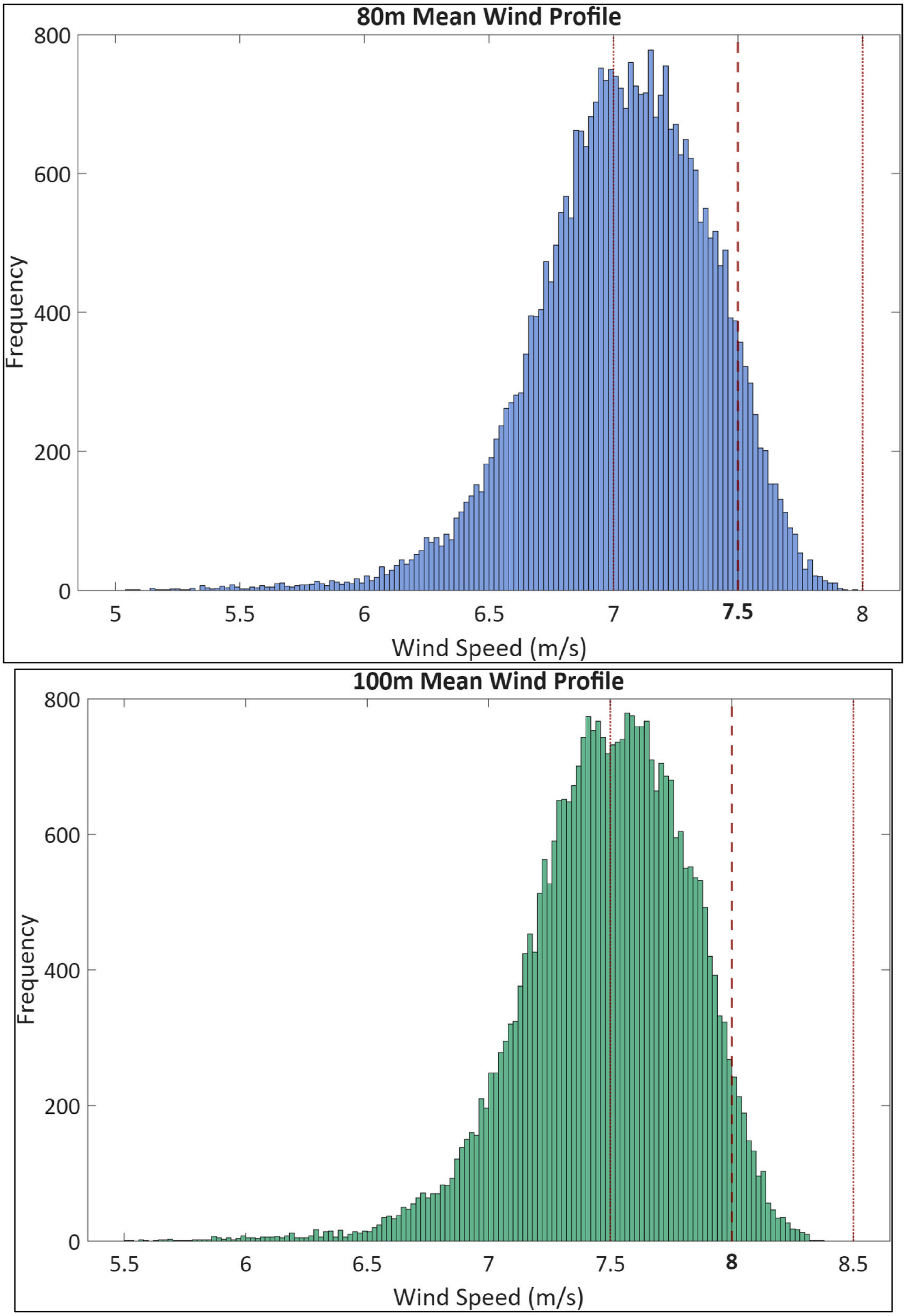


**Fig. 5.** Statewide histograms of mean wind speed in Iowa at 80 m and 100 m hub-height profiles, showing the adopted threshold values (7.5 m/s and 8.0 m/s) and their ± 0.5 m/s sensitivity ranges used for wind-suitability screening.

Equation (8):

$$P = \frac{\rho A V^3}{2} \qquad \text{Eq. 8}$$

where $P$ is power, $\rho$ air density, $A$ is rotor-swept area, and $V$ mean wind speed ([74]; Hasan et al., 2017; Hansen, 1992). Within the 80 m sensitivity range (7–8 m/s), the theoretical available power increases by 49 % ($(8^3/7^3) = 1.493$), illustrating how modest changes near the chosen thresholds translate into significant improvements in turbine output and economic performance. Thus, the final thresholds of 7.5 m/s (at 80 m) and 8.0 m/s (at 100 m) integrate both engineering standards and Iowa-specific climatological evidence, ensuring physically justified and spatially consistent site selection. These relationships are shown in Fig. 5, where the ±0.5 m/s sensitivity belts illustrate the dense, high-efficiency zones adopted for screening.

Lastly, we checked the wind-turbine locations to prevent intersection between these potential sites and existing installations. The existing turbine buffers were removed from candidate areas to avoid conflicts in energy generation and land use, ensuring that all newly identified regions represent truly independent sites. The 1,000m buffer was adopted as an upper-bound setback to maintain both aerodynamic and hydrologic consistency within the spatial framework of this study. From a design perspective, inter-turbine spacing guidelines generally recommend 5–10 rotor diameters in the prevailing wind direction and 3–5 diameters laterally ([75]; [74]), which corresponds to approximately 600–1,400m for modern utility-scale turbines with rotor diameters of 120–140m. The adopted 1 km distance therefore lies near the middle of this accepted design range, providing a conservative margin that limits wake interactions, turbulence intensity, and structural fatigue for both existing and prospective turbines.

In addition to its aerodynamic rationale, the same distance also functions as a hydrologic safety buffer, harmonizing the turbine-spacing logic with the flood-risk dimension of the analysis. In Iowa's low-relief terrain, floodwaters can propagate laterally across wide plains, and in some regions, overbank inundation may extend hundreds of meters beyond mapped flood boundaries. By maintaining a 1 km offset, potential siting areas remain secure even under extreme lateral flood expansion scenarios, preserving the hydrologic integrity of future installations. This dual-purpose setback ensures that candidate locations retain aerodynamic independence, operational efficiency, and flood safety within a single, unified spatial criterion.

## 3. Results and discussion

A comprehensive examination of correlation assessments and statistical data reveals important connections between elevation changes, flood risk, wind turbine vulnerability, and drainage capacity in Iowa. This multifaceted study provides a robust foundation for designing mitigation strategies and strengthening wind energy systems against flooding while emphasizing the requirements to consider drainage dynamics in future planning efforts.

### 3.1. Elevation analysis for wind turbine areas

Fig. 6 shows the average elevation for the different buffer zones, showing critical factors such as mean elevation, range, variance, and standard deviation. This analysis examines the relationship between zonal statistic findings across expanding buffer zones and flood occurrence (including flood depth), providing insight into how flood risk evolves with expansion area. The observed trends inform the final assessment of suitable sites, allowing for comparison against existing wind turbine locations to determine whether the selected areas exhibit improved flood resilience.

As shown in Fig. 6, the average elevation for buffer zones decreases consistently with expansion distance. The rate of decrease,

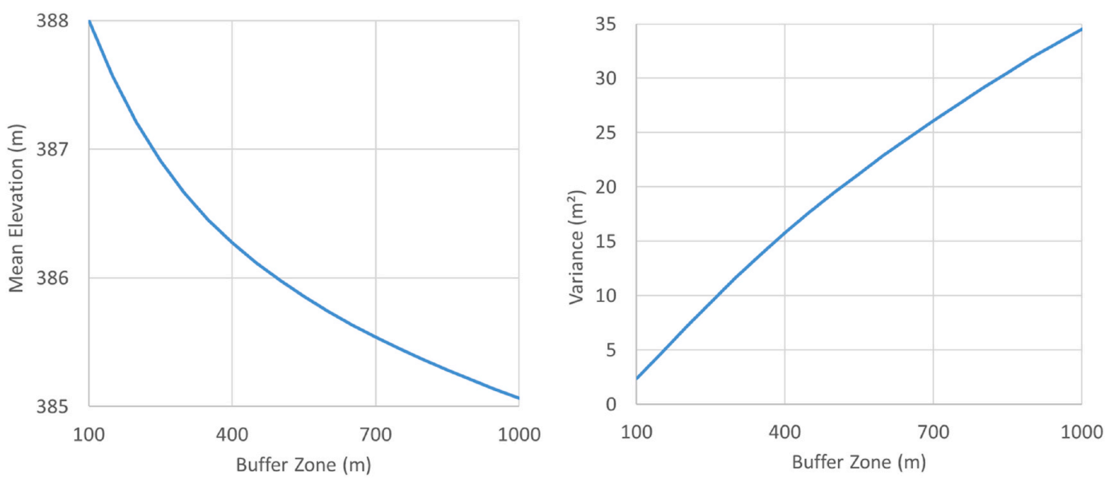


**Fig. 6.** Mean elevation and elevation variance averaged across all turbines for each buffer zone distance.

however, gradually slows as the buffer grows larger, producing a smooth nonlinear trend rather than a sharp decline. This pattern reflects the common placement of turbines at higher elevations, where the surrounding terrain gently flattens outward. Because the turbines are positioned on elevated points, expanding the buffer zones progressively incorporates lower but less variable terrain. As a result, variance of elevation values increases almost linearly with expansion, though the rate of increase slows slightly as the buffer widens. This behavior indicates that most of the terrain variability is captured within the general surroundings of the turbines, and beyond that, elevation differences contribute less dramatically to the overall variation.

To visually depict the consistency of elevation variation across different buffer zones, we selected the 100m, 500m, and 1,000m buffer-zone statistical values within the same histogram. The zonal-statistics outputs from GIS allow partial cell contributions, ensuring that buffer zones do not need to align perfectly with raster cells. Instead of displaying absolute elevations, the histograms illustrate how elevation variability changes across different buffer zones, helping to compare trends rather than cumulative values. As depicted in Fig. 7, wind turbines exhibit a consistent trend of variation increase by expansion across different buffer zones. It is essential to recognize that each location and, consequently, each buffer zone expansion demonstrates unique variations in elevation. The smaller buffer zones, particularly the 100m radius, exhibit a high concentration of low-variation values due to the limited area around turbine foundations. As the buffer increases to 500m, the variation values expand toward moderate ranges, showing that the surrounding landscape introduces more topographic differences. At 1,000m, the overall distribution becomes dominant, with cumulative frequencies shifting toward higher variation ranges, illustrating how broader areas capture larger terrain gradients. This consistency underscores the robustness and reliability of the analysis across different buffer zone expansions.

### 3.2. Flood and drainage analysis for wind turbine areas

In our analysis of drainage capacity distribution for the state soil profile, we uncovered important insights into how soil permeability and water retention affect flood risk for wind turbine installations in Iowa. By looking at different buffer zones, we focus on key factors like average maximum flood depth, the number of flooded areas, and the average base soil drainage capacity, as shown in Fig. 8. This process will assist in understanding the complex relationship between the land's characteristics and the risk of flooding.

The analysis shows a gradual rise in maximum flood depth as buffer zones extend up to 300m, with a curvilinear increase continuing to 1,000m. This trend is observed for both 100-year and 500-year flood scenarios, though flood depth and the number of flooded areas is higher for the 500-year scenario across all buffer zones. Similarly, total drainage capacity follows a comparable pattern with buffer zone extension. For both flood scenarios, drainage scores reflect similar trends, though there is a slight decrease in the average drainage score for the 100-year flood scenario beyond the 950m buffer zone. This decrease is minor and does not substantially affect the overall analysis, whereas the drainage score remains stable for the 500-year flood zones. The findings indicate a strong relationship between low soil permeability and rapid flood onset since areas with poor drainage were inundated earlier. In practical terms, improving local drainage performance through actions such as subsurface drainage installation, access road grading, or regular maintenance of stormwater channels can help reduce localized inundation and protect turbine foundations during flood events. Meanwhile, areas with poor drainage were inundated earlier, showing a linear trend in the number of flooded zones. Notably, once the

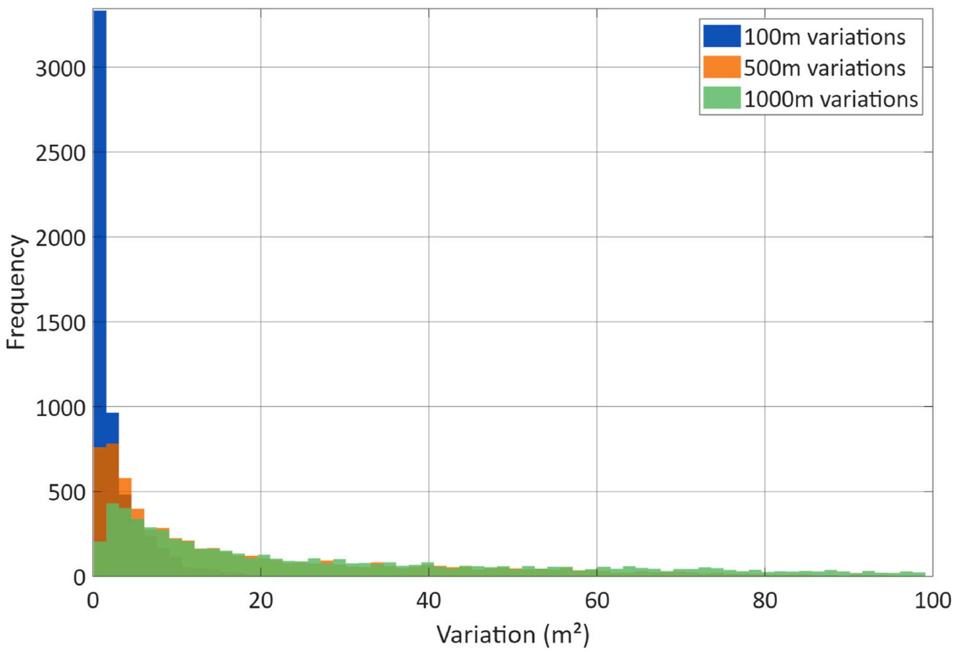


**Fig. 7.** Elevation variation histogram for 100m, 500m, and 1,000m wind turbine buffer zones.

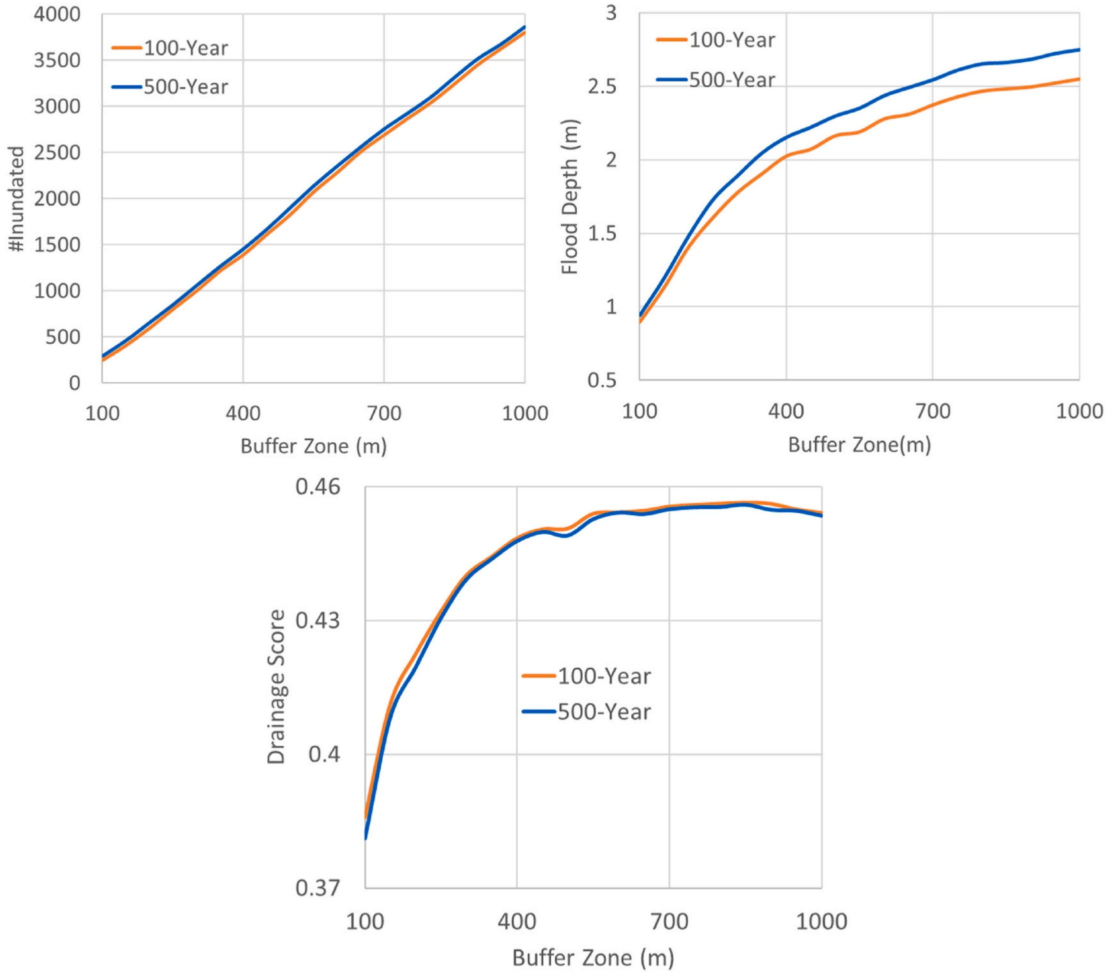


**Fig. 8.** Wind turbine buffer zone statistics; number of flooded zones (upper left), maximum flood depth (upper right), and average base soil drainage capacity (lower) for wind turbine buffer zones.

buffer zone expands beyond 850m, more than half of the turbine areas are inundated, emphasizing the cruciality for proactive mitigation measures.

Table 4 provides complementary inundation statistics, including mean depth, median depth, and flooded share, in addition to the maximum depths used in correlation analysis. These measures highlight how inundation evolves as buffer zones expand: the number of inundated buffers increases substantially, while the flooded share declines because larger zones incorporate more non-inundated areas. Mean and median depths, which remain below 0.6 m even at 1,000m, capture typical flood conditions across zones, whereas

**Table 4**
Summary of inundation characteristics by buffer zone and flood scenario.

| Flood Scenario | 100-Year | | | | |
|---|---|---|---|---|---|
| Zone | Inundated Zone (#) | Inundation Area (km$^2$) | Mean Depth (m) | Median Depth (m) | Flooded Share/Inundated Zone (%) |
| 100m | 248 | 1.81 | 0.29 | 0.31 | 23.60 |
| 500m | 1827 | 130.23 | 0.51 | 0.45 | 9.21 |
| 1000m | 3804 | 690.95 | 0.55 | 0.48 | 5.88 |
| Flood Scenario | **500-Year** | | | | |
| Zone | Inundated Zone (#) | Inundation Area (km$^2$) | Mean Depth (m) | Median Depth (m) | Flooded Share/Inundated Zone (%) |
| 100m | 290 | 2.3 | 0.35 | 0.35 | 25.71 |
| 500m | 1899 | 156.10 | 0.57 | 0.52 | 10.63 |
| 1000m | 3861 | 817.31 | 0.63 | 0.57 | 6.86 |

maximum depth reflects the most severe inundation within each buffer. We therefore used maximum depth as the input to correlation analysis to relate flood severity to terrain and soil characteristics, while employing inundation extent and flooded area metrics for site suitability and future location assessments.

### 3.3. Placement year analysis for wind turbines

Both the 100-year and 500-year flood scenarios show strong similarities in the distribution of inundation numbers and placement years for wind turbines. The average age of inundated wind turbine areas will be displayed for both scenarios in a single graph in Fig. 10. However, the distribution of placement years is nearly identical. So, in order to streamline the analysis and avoid redundancy, only the 100-year flood scenario is shown for the distribution of placement years in Fig. 9.

As shown in Fig. 9, most of Iowa's wind turbines were installed between 2016 and 2023, accounting for nearly half of all turbines statewide (2982 out of 6345). This same group represents the majority of flood-exposed turbines across all buffer distances. Older installations (1990s–2000s) show notably lower exposure rates, reflecting their concentration in less flood-prone regions. Fig. 10 shows that the average age of Iowa wind turbines is 10.68 years, whereas the average age of inundated turbines ranges from about 8.83 years at the 100m buffer to 9.75 years at 1,000m for both flood scenarios. The gradual increase with buffer size reflects the inclusion of slightly older installations as the spatial extent expands, yet the average age of affected turbines remains consistently lower than the statewide mean. This pattern suggests that recent development has expanded into more hydrologically sensitive zones, reinforcing the need to integrate flood risk metrics into site selection and permitting to improve the long-term resilience of new installations.

### 3.4. Correlation for flooding and terrain characteristics

In this phase, we investigated the correlations between flood conditions and the related elevation and drainage statistics. Table 5 presents the pairwise Pearson correlation coefficients with 95 % confidence intervals, based on $n = 19$ observations corresponding to each successive buffer zone expansion (100–1,000m).

The correlations with elevation-based variables are very high ($|r| > 0.95$) with narrow confidence intervals. Flood depth and flooded areas increase in near-proportional alignment with elevation variance, elevation standard deviation, and mean elevation. The strong negative correlations with mean elevation ($r \approx -0.99$) reflect the expected pattern of greater flood depth and extent in lower-lying terrain. These values represent cross-scale associations between flood exposure and terrain variability as buffer zones expand. Such near-perfect coefficients arise because both flood and terrain metrics increase monotonically with buffer radius, yet their magnitude shows that the rates of increase are closely aligned rather than independent. However, the soil drainage variable behaves differently. The correlation between flooded areas and mean drainage is relatively lower and the confidence interval is wider. The soil drainage variable also demonstrates strong correlation with flood metrics ($r \approx 0.95$ for flood depth, $r \approx 0.78$ for flooded area). These values remain high, though the wider confidence interval indicates that proportionality with buffer expansion is less tight compared to elevation measures. This reflects the categorical and spatially heterogeneous nature of soil drainage classes. Once poorly drained areas

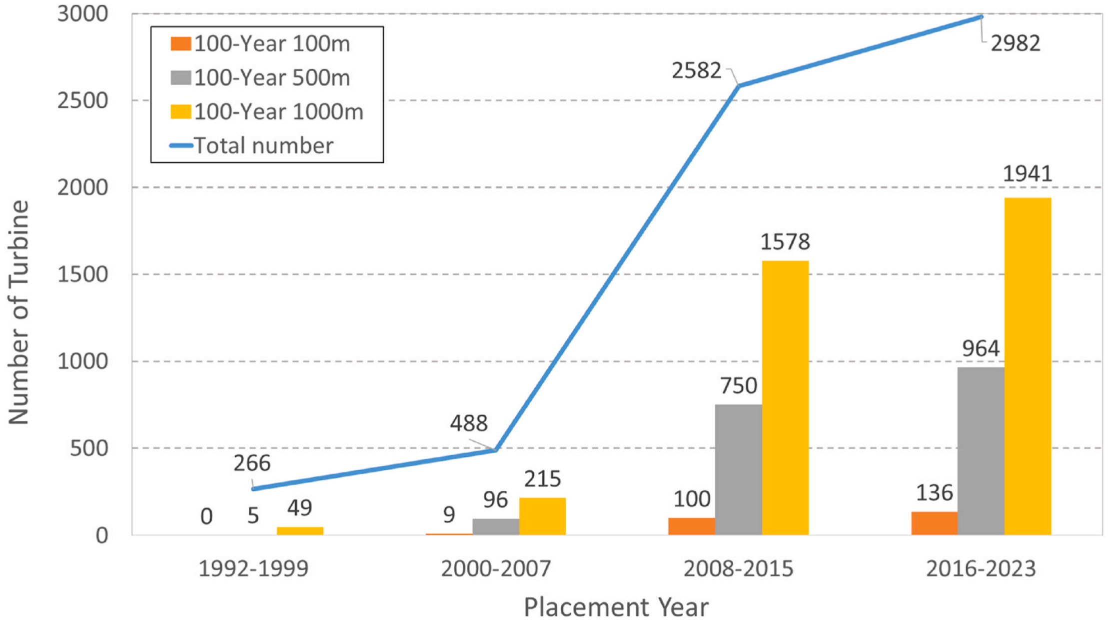


**Fig. 9.** Distribution of placement years for Iowa's wind turbines and their inundation cases under 100-year flood conditions, with 100m, 500m, and 1,000m buffer zone extensions.

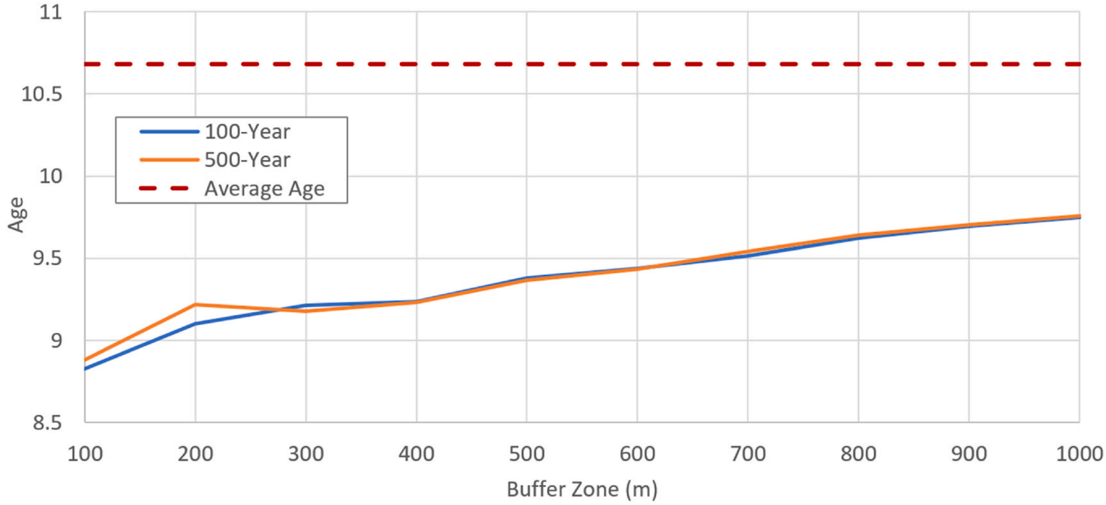


**Fig. 10.** The average age of inundated wind turbine areas for 100-year and 500-year flood scenarios, compared across various buffer zone extensions from the Iowa Wind Turbine Inventory.

**Table 5**
Pairwise Pearson correlation results for flood vulnerability (n = 19 buffer zones).

| Correlation Pairs | 100-year | 500-year |
|---|---|---|
| Flood Depth - Elevation Variance | 0.959 [0.895–0.985] | 0.961 [0.899–0.985] |
| Flood Depth – Elevation (σ) | 0.987 [0.965–0.995] | 0.988 [0.968–0.995] |
| Flood Depth - Mean Elevation | −0.995 [(-0.986)–(-0.998)] | −0.995 [(-0.988)–(-0.998)] |
| Flood Depth - Drainage | 0.953 [0.880–0.982] | 0.950 [0.871–0.981] |
| Flooded Count - Elevation Variance | 0.996 [0.989–0.998] | 0.996 [0.989–0.999] |
| Flooded Count - Elevation (σ) | 0.977 [0.939–0.991] | 0.977 [0.940–0.991] |
| Flooded Count - Mean Elevation | −0.961 [(-0.899)–(-0.985)] | −0.962 [(-0.901)–(-0.985)] |
| Flooded Count - Drainage | 0.786 [0.515–0.914] | 0.783 [0.510–0.913] |

are intersected, further buffer expansion often incorporates similar classes, which reduces proportionality without eliminating the underlying association.

These results are based on 19 wind turbine buffer-zone averages, obtained by aggregating values across all turbines at each buffer radius. This approach was chosen to capture statewide cross-scale trends to show how flood metrics and terrain descriptors co-vary as buffer zones expand. Flooding in uneven terrain can undermine turbine foundations, restrict maintenance access, and accelerate structural deterioration through prolonged saturation. Similarly, poor soil drainage can delay site recovery after flood events, prolonging operational downtime. The inclusion of confidence intervals supports the statistical reliability of these aggregated correlations despite the limited number of increments. Overall relationships highlight that elevation-based variables are the strongest predictors of flood exposure, with terrain variability providing a consistent indicator of susceptibility across spatial scales. Moreover, soil drainage adds complementary but more localized insights, reflecting site-specific hydrologic responses. From a planning perspective, this means that regional or statewide screening for new turbine sites can primarily rely on topographic indicators to identify high-risk zones, while drainage characteristics should be integrated at the detailed design or permitting stage to fine-tune construction layouts and access routes. Together, these parameters form a scalable framework that supports predictive flood-risk mapping and resilient infrastructure planning for Iowa's growing wind-energy network.

### *3.5. Statewide inundation impact assessment*

In Fig. 11, we have delineated the inundated areas for the 100m, 500m, and 1,000m buffer zones under the 100-year flooding scenario. This visualization assists in illustrating how these zones relate to each other and the extent of flooding. While we analyzed both the 100-year and 500-year scenarios, we decided to visualize only 100-year results since overall distribution remains relatively similar between these flooding scenarios. For instance, in the 100m buffer zone expansion, the difference in inundation between the two flood scenarios is 42 wind turbines, which means a 17 % increase. On the other hand, in the 500m zone, the difference is 72 wind turbines, representing a 4 % increase, and in the zone of 1,000m, which is our maximum expansion, the difference drops to 52 wind turbines, representing only a 1.5 % total increase. With thousands wind turbine locations in our case study area, it can be challenging to distinguish the differences due to the accumulation of points.

As depicted in Fig. 11, it becomes clear that the northern region of Iowa is particularly vulnerable to flooding on wind turbines,

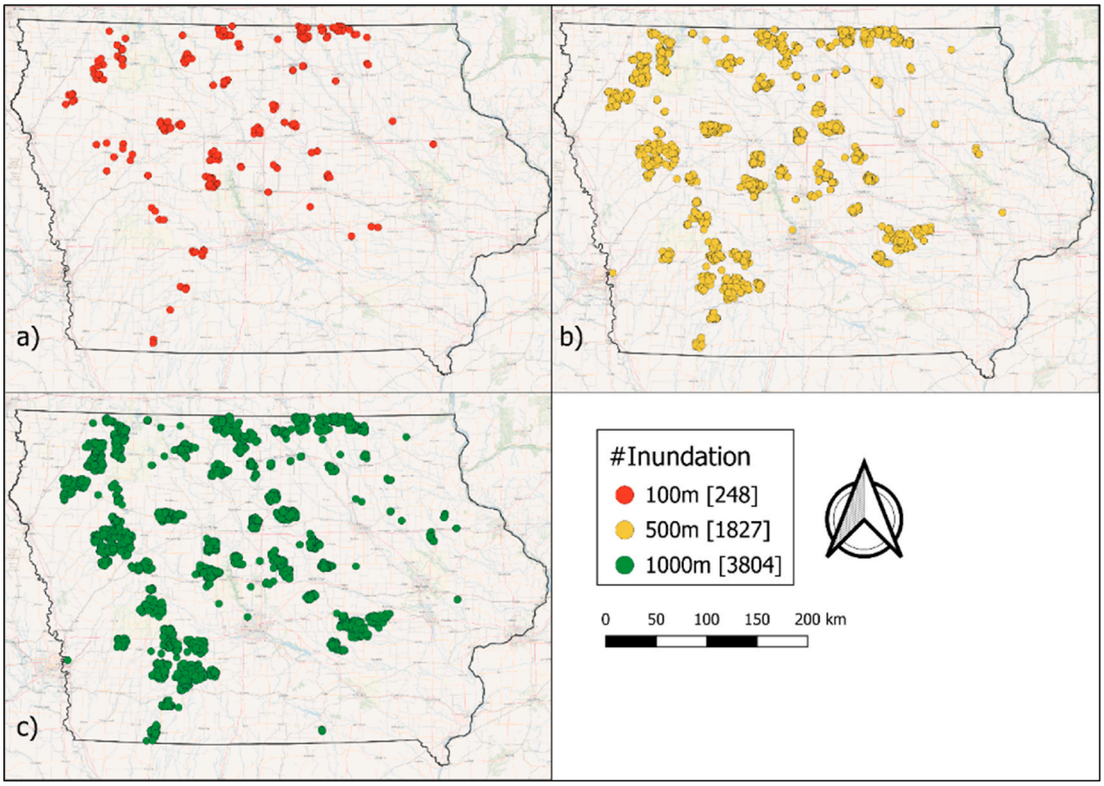


**Fig. 11.** Overall inundated locations for 100m, 500m and 1,000m buffer zone in 100-year flood scenario of Iowa wind turbines.

especially in the smaller buffer zones. When the buffer expands to 500m, even higher elevations, especially in midwestern Iowa, show increased exposure due to the significant elevation changes and moderate drainage capacity in the area. In both flood scenarios, about 5 percent of all Iowa wind turbines are affected in the base −100m-buffer zone. This percentage rises dramatically to 30 percent at the 500m extension and a staggering 61 % with a 1,000m extension.

As mentioned earlier, a similar trend appears both in the 100-year and 500-year flood scenarios, highlighting a consistent vulnerability. This pattern underscores a persistent exposure, showing that floods are a significant threat to wind turbines in Iowa, regardless of how intense the flooding may be. Table 6 summarizes these statewide inundation exposure levels and places them in the context of statistical uncertainty. Exposure grows quickly with buffer expansion: only a small share of turbines is inundated at 100m, but this increases to nearly one-third by 500m and over 60 percent by 1,000m. Because the dataset covers 6345 turbines distributed across 55 HUC-8 watersheds, we assessed uncertainty at two levels. Resampling at the turbine level (N = 6345) produces very narrow confidence intervals, showing that the statewide averages are statistically stable. For example, the 100m buffer under the 100-year flood produces an exposure estimate of 248 turbines, with a 95 % CI of ranging from 3.44 to 4.41 percent. In contrast, resampling at the watershed level (N = 55) produces wider confidence intervals, such as from 2.68 to 5.40 percent for the same scenario. This difference reflects the clustered nature of turbine distributions: while the average statewide exposure is robust, localized flooding in a

**Table 6**
Statewide wind turbine inundation exposure under 100-year and 500-year flood scenarios for three buffer distances (100m, 500m, and 1,000m). Results include the number and percentage of inundated turbines, along with 95 % confidence intervals derived from turbine-level and HUC-8 bootstrap resampling.

| Flood Scenario | 100-year Flood | | | |
|---|---|---|---|---|
| Zone | #Inundated | %Inundated | 95 % CI (Turbine) | 95 % CI (HUC-8) |
| 100m | 248 | 3.91 | 3.44–4.41 | 2.68–5.40 |
| 500m | 1827 | 28.79 | 27.60–29.91 | 24.98–32.78 |
| 1,000m | 3804 | 59.95 | 58.72–61.17 | 55.86–64.85 |
| **Flood Scenario** | **500-year Flood** | | | |
| **Zone** | **#Inundated** | **%Inundated** | **95 % CI (Turbine)** | **95 % CI (HUC-8)** |
| 100m | 290 | 4.67 | 4.04–5.09 | 3.08–6.33 |
| 500m | 1899 | 29.93 | 28.81–31.11 | 26.24–34.26 |
| 1,000m | 3861 | 60.85 | 59.62–61.99 | 56.38–65.78 |

few watersheds can shift the results significantly. Reporting both perspectives highlights that flood hazards are not evenly distributed, and that hydrologic dependence can magnify local impacts.

According to the findings provided in Tables 6 and 7, there is a clear relationship between the capacity exposure scenarios for 100-year and 500-year flood events. The impact of flooding on energy capacity appears to be minor within a 100m buffer area, as it only accounts for less than 5 % of wind energy capacity in both flood scenarios. However, as the buffer zone size increases, the impact becomes more significant. With a 500m buffer area extension, the exposed energy percentage climbs to over 30 %, and for a 1,000m buffer extension, which is the largest buffer zone we evaluated, exceeds 60 % in both 100-year and 500-year flood scenarios. Additionally, a consistent pattern emerges across all three sample buffer zone sizes and both flood scenarios. The percentage of capacity exposure is always slightly higher than the percentage of inundated wind turbine zones. Although the overall percentage of capacity exposed is greater than the percentage of inundation, the larger capacities of the inundated turbines amplify the impact. This concentration suggests that even moderate flooding could disproportionately affect statewide generation potential. Integrating these exposure statistics into energy-resilience planning can help utilities prioritize reinforcement, improve access routes, and develop curtailment protocols during flood alerts, highlighting the need to evaluate both spatial extent and generation capacity in future siting and mitigation efforts.

### 3.6. Suitable locations for new wind turbine placement

In this study, we implemented rectangular parcels for evaluating potential wind turbine locations, matching our maximum buffer zone, a 1,000m. This dimension was chosen to match the diameter of the largest buffer zone considered, which helps maintain a consistent and systematic analysis approach. Fig. 12 presents potential wind turbine sites, focusing on areas with steady wind conditions at altitudes of 80m and 100m. It also excludes regions with existing structures and those at risk of flooding, ensuring that only the most suitable locations are highlighted.

Despite the higher density of existing wind turbines, western Iowa remains the most favorable region for future installations. This area consistently exhibits the strongest wind resources statewide while also showing minimal flood exposure according to the statewide inundation results. The combination of stable wind patterns, higher elevations, and lower hydrologic vulnerability offsets the concentration of existing turbines, confirming its continued suitability for development. Although there are other potential sites for 80-m wind turbines, these turbines require lower wind speeds to operate effectively compared to those at 100-m. Elevating the turbine from 80 m to 100 m would increase wind speed by 4.6 % and enhance power output by 14 % [76]. This indicates that, while placing taller turbines is more complex, it offers substantial advantages in terms of cost-efficiency and energy production. Our analysis shows that more than 70 % of the chosen sites have less elevation variation compared to the average within our 1,000m buffer zone. This characteristic further confirms the suitability of these locations for new wind turbine installation, ensuring both stability and efficiency in wind energy production.

### 3.7. Limitations

While this study provides a comprehensive statewide assessment of flood exposure and site suitability for wind turbines in Iowa, several limitations should be acknowledged. First, the analysis relies on static flood scenarios from the Iowa Flood Center (IFC) and Iowa Geospatial Data Clearinghouse (IGDC), representing modeled 100-year and 500-year return periods. These datasets are based on hydrodynamic simulations that, while robust, are subject to modeling assumptions, boundary simplifications, and potential spatial gaps between HUC-8 watersheds. Inundation depths represent maximum values within floodplain boundaries, not temporal averages or dynamic hydrographs. Vertical datum inconsistencies and localized model calibration limits may introduce small errors in elevation-based comparisons.

Moreover, this study deliberately focused on flood and wind-resource interactions, excluding other spatial criteria, such as slope, land cover, grid proximity, or environmental exclusions. While this focused scope strengthens clarity and interpretability, it simplifies the complex decision environment that actual developers face. As a result, the presented suitability zones should be considered as hydrologically and aerodynamically favorable areas, not definitive development sites.

Additionally, the capacity-exposure results quantify the installed capacity located within flood-prone zones but do not translate to actual energy production loss. Real-time output depends on wind conditions, grid curtailment, and flood duration, none of which were available at the temporal resolution required for accurate energy disruption modeling. Therefore, the results should be interpreted as potential capacity at risk rather than guaranteed generation loss.

Finally, the statewide scale of this study required the aggregation of 6345 turbines and 19 buffer radii, which unavoidably generalizes local structural or geotechnical characteristics. Factors such as foundation design, drainage systems, soil reinforcement, and substation elevation were not explicitly modeled but may strongly influence site-specific resilience. Consequently, the findings provide relative vulnerability indicators rather than deterministic damage predictions.

## 4. Conclusion

In summary, this study is very instrumental in offering invaluable insights into how vulnerable wind turbines in Iowa are to flooding, intending to fill the existing gap in knowledge on the resilience of this state's energy infrastructure. By integrating elevation variability, drainage capacity, and modeled flood depth with spatial distributions of existing wind turbines, the analysis reveals clear spatial patterns of vulnerability across diverse physiographic regions.

**Table 7**
Statewide wind turbine capacity exposure under 100-year and 500-year flood scenarios for three buffer distances (100m, 500m, and 1,000m).

| Flood Scenario | 100-year Flood | |
|---|---|---|
| Zone | **Capacity Exposure (MW)** | **Capacity Exposure (%)** |
| 100m | 536.00 | 4.20 |
| 500m | 3900.60 | 30.53 |
| 1,000m | 8004.80 | 62.66 |
| Flood Scenario | **500-year Flood** | |
| Zone | **Capacity Exposure (MW)** | **Capacity Exposure (%)** |
| 100m | 626.10 | 4.90 |
| 500m | 4059.20 | 31.78 |
| 1,000m | 8118.80 | 63.56 |

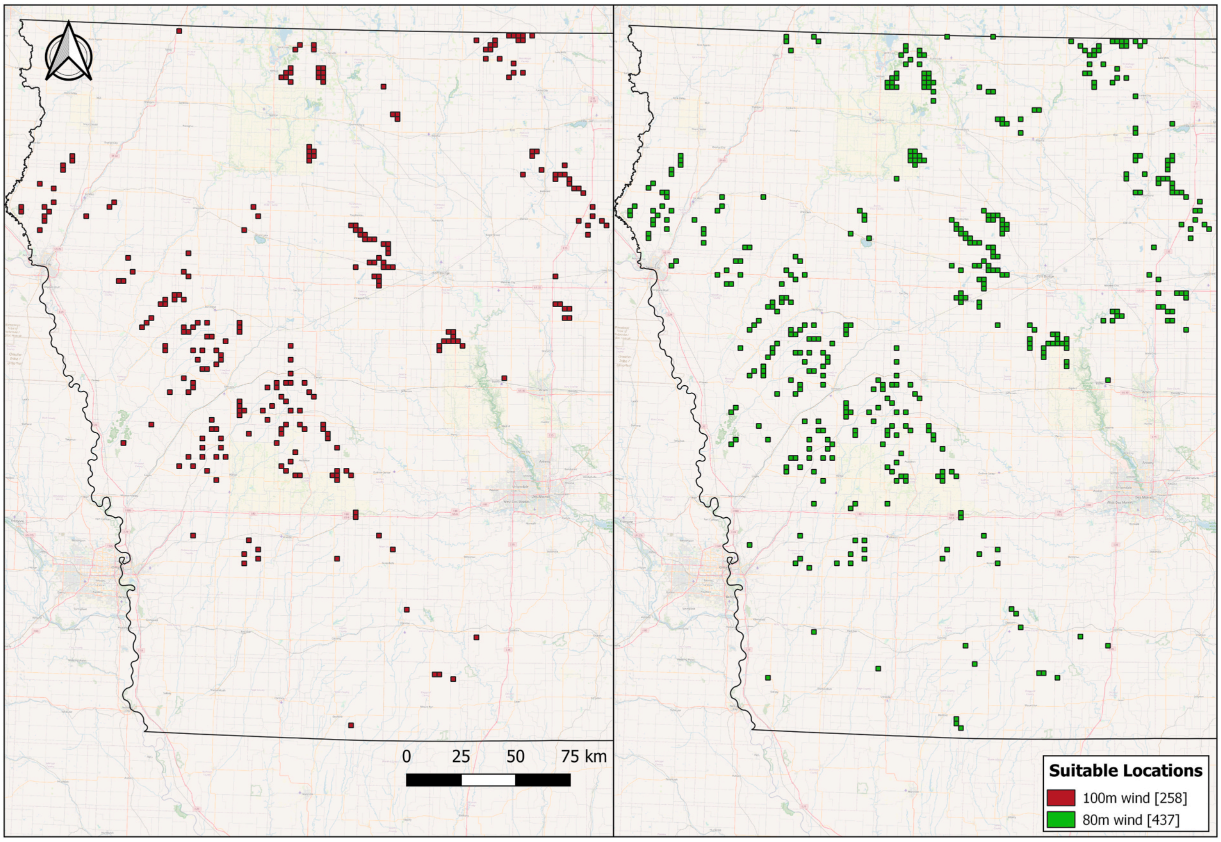


**Fig. 12.** Potential wind turbine locations for steady winds at 100m and 80m altitudes, excluding areas with occupancy and flooding risks.

Through a robust methodology encompassing zonal statistics, correlation analysis, and geospatial mapping, we uncover spatial patterns of vulnerability across diverse physiographic regions. Our findings reveal a significant correlation between elevation variance, flood risk, and wind turbine vulnerability, underscoring the need for targeted interventions to bolster resilience. From the northern region to the mid-west side of Iowa, the heightened susceptibility of wind turbines highlights the urgency of proactive measures to mitigate flood impact.

Our study on understanding the flood impacts on wind turbine capacity provides insightful information on the relationship between turbine regions and flood risks. As protective buffer zones expand, more turbines are impacted; yet we observed that turbines located in flood-prone regions typically have more energy capacity than the turbines located outside of these zones. Consequently, total energy output can be noticeably reduced even in a rather small area affected by floods. To mitigate this, we applied flood safety criteria to pinpoint locations for new turbines that are not only resilient to flooding but also positioned to harness efficient wind energy. By incorporating optimal wind speeds at dominant hub heights, we identified several promising areas, especially in western Iowa, that meet these conditions without overlapping with existing turbines, ensuring their long-term viability.

Overall, our research contributes scientific understanding while translating findings into actionable strategies to safeguard Iowa's renewable energy infrastructure. By fostering community resilience and promoting sustainability, we support a future where renewable energy remains a cornerstone of Iowa's energy system, resilient against floods and other environmental challenges.

### 4.1. Future work

Future research should extend this framework both technically and strategically. On the technical side, advancing toward dynamic, time-dependent flood–energy models would allow quantification of temporary capacity losses and recovery times during extreme events. Developing turbine-specific depth-damage and disruption curves, incorporating flood duration, soil saturation, and electrical component sensitivity, will refine impact estimates and support probabilistic risk analyses. Integrating nonstationary hydrologic models with projected precipitation and land-use trends will further improve prediction accuracy under changing climate conditions.

Expanding the geospatial database to include slope, aspect, land-cover type, grid proximity, and access-road connectivity will strengthen multi-criteria decision analyses (MCDM) for site selection. A hybrid framework that couples quantitative filtering (as used here) with weighted MCDM ranking could balance environmental, infrastructural, and socioeconomic considerations. Moreover, examining turbines that remained operational during past floods can yield empirical insights into resilient siting and design practices, improving predictive modeling and validation.

From an operational and policy perspective, future studies should evaluate accessibility and maintenance disruptions during floods to identify remote wind farms vulnerable to temporary isolation. Scenario testing for alternative recurrence intervals (e.g., 50-year or compound flood events) would help define adaptive management thresholds. Policymakers and energy agencies could apply these results to guide flood-resilient zoning, infrastructure reinforcement incentives, and renewable-energy permitting standards that integrate flood safety into the planning and approval process.

Finally, integrating socioeconomic impact analyses, such as electricity-demand shifts, repair cost estimation, and service interruption mapping, will connect physical exposure with community and economic resilience outcomes. By combining dynamic modeling, expanded spatial criteria, and policy frameworks, future research can build a comprehensive, data-driven foundation for safeguarding Iowa's renewable-energy infrastructure against evolving hydrological extremes.

## CRediT authorship contribution statement

**Ege Duran:** Writing – original draft, Visualization, Validation, Investigation, Formal analysis, Data curation. **Ibrahim Demir:** Writing – review & editing, Validation, Supervision, Investigation.

## Declaration of competing interest

The authors declare that they have no known competing financial interests or personal relationships that could have appeared to influence the work reported in this paper.

## Data availability

Data will be made available on request.

## References

[1] S. Fazeli, T.H. Rashidi, M. Mojtahedi, M. Haghani, Measuring individual preparedness for flood and bushfire emergencies, Int. J. Disaster Risk Reduct. (2025) 105651, https://doi.org/10.1016/j.ijdrr.2025.105651.
[2] J.M. Sadler, N. Haselden, K. Mellon, A. Hackel, V. Son, J. Mayfield, J.L. Goodall, Impact of sea-level rise on roadway flooding in the Hampton Roads region, Virginia, J. Infrastruct. Syst. 23 (4) (2017) 05017006, https://doi.org/10.1061/(ASCE)IS.1943-555X.0000397.
[3] B.A. Cikmaz, E. Yildirim, I. Demir, Flood susceptibility mapping using fuzzy analytical hierarchy process for Cedar Rapids, Iowa, Int. J. River Basin Manag. (2023) 1–13, https://doi.org/10.31223/X57344.
[4] I. Haltas, E. Yildirim, F. Oztas, I. Demir, A comprehensive flood event specification and inventory: 1930–2020 Turkey case study, Int. J. Disaster Risk Reduct. 56 (2021) 102086, https://doi.org/10.1016/j.ijdrr.2021.102086.
[5] M. Borowska-Stefańska, S. Wiśniewski, M.T. Andrei, Accessibility to places of evacuation for inhabitants of flood-prone areas in Mazovia Province, Geomatics Environ. Eng. 11 (2017) 31–47, https://doi.org/10.7494/geom.2017.11.3.31.
[6] T.K. McDermott, Global exposure to flood risk and poverty, Nat. Commun. 13 (1) (2022) 3529, https://doi.org/10.1038/s41467-022-30725-6.
[7] S.E. Crawford, M. Brinkmann, J.D. Ouellet, F. Lehmkuhl, K. Reicherter, J. Schwarzbauer, H. Hollert, Remobilization of pollutants during extreme flood events poses severe risks to human and environmental health, J. Hazard Mater. 421 (2022) 126691, https://doi.org/10.1016/j.jhazmat.2021.126691.
[8] Mohamed Farook Kalendher Lebbe, Weena Lokuge, Sujeeva Setunge, Kevin Zhang, Failure mechanisms of bridge infrastructure in an extreme flood event, in: Proceedings of the 1st International Conference on Infrastructure Failures and Consequences, 2014, pp. 124–132.
[9] Z. Li, I. Demir, A comprehensive web-based system for flood inundation map generation and comparative analysis based on height above nearest drainage, Sci. Total Environ. 828 (2022) 154420, https://doi.org/10.1016/j.scitotenv.2022.154420.
[10] E. Duran, Y. Alabbad, J. Mount, E. Yildirim, I. Demir, Comprehensive analysis of riverine flood impact on bridge and transportation network: iowa case study, Int. J. River Basin Manag. (2025) 1–14, https://doi.org/10.1080/15715124.2025.2457546.
[11] Z. Li, F.Q. Duque, T. Grout, B. Bates, I. Demir, Comparative analysis of performance and mechanisms of flood inundation map generation using height above nearest drainage, Environ. Model. Software 159 (2023) 105565, https://doi.org/10.1016/j.envsoft.2022.105565.
[12] A. Martinez, G. Iglesias, Wind resource evolution in Europe under different scenarios of climate change characterised by the novel shared socioeconomic pathways, Energy Convers. Manag. 234 (2021) 113961, https://doi.org/10.1016/j.enconman.2021.113961.

[13] Y. Zhang, J. Han, G. Pan, Y. Xu, F. Wang, A multi-stage predicting methodology based on data decomposition and error correction for ultra-short-term wind energy prediction, J. Clean. Prod. 292 (2021) 125981, https://doi.org/10.1016/j.jclepro.2021.125981.
[14] M. Rezaei-Shouroki, The location optimization of wind turbine sites with using the MCDM approach: a case study, Energy Equip. Syst. 5 (2) (2017) 165–187, https://doi.org/10.22059/ees.2017.25757.
[15] S. Grassi, N. Chokani, R.S. Abhari, Large scale technical and economical assessment of wind energy potential with a GIS tool: case study Iowa, Energy Policy 45 (2012) 73–85, https://doi.org/10.1016/j.enpol.2012.01.061.
[16] G. Hou, K. Xu, J. Lian, A review on recent risk assessment methodologies of offshore wind turbine foundations, Ocean. Eng. 264 (2022) 112469, https://doi.org/10.1016/j.oceaneng.2022.112469.
[17] J. Pasqualetti Martin, Opposing wind energy landscapes: a search for common cause, Ann. Assoc. Am. Geogr. 101 (4) (2011) 907–917, https://doi.org/10.1080/00045608.2011.568879.
[18] F. Porté-Agel, M. Bastankhah, S. Shamsoddin, Wind-turbine and wind-farm flows: a review, Boundary-Layer Meteorol. 174 (1) (2020) 1–59, https://doi.org/10.1007/s10546-019-00473-0.
[19] Iowa Environmental Council, Iowa wind energy fact sheet. www.iaenvironment.org, 2023.
[20] E. Yildirim, Y. Alabbad, I. Demir, Non-structural flood mitigation optimization at community scale: middle cedar case study, J. Environ. Manag. 346 (2023) 119025, https://doi.org/10.1016/j.jenvman.2023.119025.
[21] K. Gkritza, D.E. Smith, R.B. Sperry, I. Nlenanya, W. Jiang, *Iowa's Renewable Energy and Infrastructure Impacts* (No. IHRB Project TR-593), Iowa. Dept. of Transportation, 2010.
[22] I. Demir, Z. Xiang, B. Demiray, M. Sit, Waterbench: a large-scale benchmark dataset for data-driven streamflow forecasting, Earth Syst. Sci. Data Discuss. 2022 (2022) 1–19, https://doi.org/10.5194/essd-14-5605-2022.
[23] M. Sit, B.C. Seo, I. Demir, Iowarain: a statewide rain event dataset based on weather radars and quantitative precipitation estimation, arXiv:2107.03432 (2021), https://doi.org/10.48550/arXiv.2107.03432.
[24] Z. Li, Z. Xiang, B.Z. Demiray, M. Sit, I. Demir, MA-SARNet: a one-shot nowcasting framework for SAR image prediction with physical driving forces, ISPRS J. Photogrammetry Remote Sens. 205 (2023) 176–190, https://doi.org/10.1016/j.isprsjprs.2023.10.002.
[25] USGS, Floods of May 30 to June 15, 2008, in the Iowa River and Cedar River Basins, Eastern Iowa, 2010.
[26] C.F. Mutel (Ed.), A Watershed Year: Anatomy of the Iowa Floods of 2008, University of Iowa Press, 2010, https://doi.org/10.2307/j.ctt20mvd5n.
[27] N. Tabasi, M. Fereshtehpour, B. Roghani, A review of flood risk assessment frameworks and the development of hierarchical structures for risk components, Discover Water 5 (1) (2025), https://doi.org/10.1007/s43832-025-00193-2. Article 10.
[28] A.J. Peck, S.L. Adams, A.K. Armstrong, M.L. Bartlett, M.L. Bortman, A.B. Branco, E. Smith, A new framework for flood adaptation: introducing the flood adaptation hierarchy, Ecol. Soc. 27 (4) (2022) 5, https://doi.org/10.5751/ES-13544-270405.
[29] Y. Alabbad, E. Yildirim, I. Demir, A web-based analytical urban flood damage and loss estimation framework, Environ. Model. Software 163 (2023) 105670, https://doi.org/10.2139/ssrn.4358329.
[30] Y. Alabbad, I. Demir, Understanding flood risk in public transit systems: insights from accessibility and vulnerability analysis in Iowa, Int. J. Disaster Risk Reduct. (2025) 105615, https://doi.org/10.1016/j.ijdrr.2025.105615.
[31] C.A. Grant, Y. Alabbad, E. Yildirim, I. Demir, Comprehensive assessment of flood risk and vulnerability for essential facilities: iowa case study, Urban Sci. 8 (3) (2024) 145, https://doi.org/10.3390/urbansci8030145.
[32] E. Yildirim, C. Just, I. Demir, Flood risk assessment and quantification at the community and property level in the State of Iowa, Int. J. Disaster Risk Reduct. 77 (2022) 103106, https://doi.org/10.1016/j.ijdrr.2022.103106.
[33] Y. Alabbad, I. Demir, Comprehensive flood vulnerability analysis in urban communities: iowa case study, Int. J. Disaster Risk Reduct. 74 (2022) 102955, https://doi.org/10.1016/j.ijdrr.2022.102955.
[34] T. Tanir, E. Yildirim, C.M. Ferreira, I. Demir, Social vulnerability and climate risk assessment for agricultural communities in the United States, Sci. Total Environ. 908 (2024) 168346, https://doi.org/10.1016/j.scitotenv.2023.168346.
[35] A.M. Elmoustafa, Neveen Y. Saad, Ehab M. Fattouh, Defining the degree of flood hazard using a hydrodynamic approach, a case study: wind turbines field at west of Suez Gulf, Ain Shams Eng. J. 11 (3) (2020) 741–749, https://doi.org/10.1016/j.asej.2019.12.005. ISSN 2090-4479.
[36] G.Y. Zou, Toward using confidence intervals to compare correlations, Psychol. Methods 12 (2007) 399–413, https://doi.org/10.1037/1082-989X.12.4.399.
[37] P. Michel, C. Butenweg, S. Klinkel, Pile-grid foundations of onshore wind turbines considering soil-structure-interaction under seismic loading, Soil Dynam. Earthq. Eng. 109 (2018) 299–311, https://doi.org/10.1016/j.soildyn.2018.03.009.
[38] A.F. Jacobson, D.L. Mauzerall, J.D. Jenkins, Quantifying the impact of energy system model resolution on siting, cost, reliability, and emissions for electricity generation, Environ. Res.: Energy 1 (3) (2024) 035009, https://doi.org/10.1088/2753-3751/ad6d6f.
[39] A. Sotoudeh-Anvari, The applications of MCDM methods in COVID-19 pandemic: a state of the art review, Appl. Soft Comput. 126 (2022) 109238, https://doi.org/10.1016/j.asoc.2022.109238.
[40] M. Sanchez Gomez, J.K. Lundquist, The effect of wind direction shear on turbine performance in a wind farm in central Iowa, Wind Energy Science 5 (1) (2020) 125–139, https://doi.org/10.5194/wes-5-125-2020.
[41] M.R. Milligan, T. Factor, Optimizing the geographic distribution of wind plants in Iowa for maximum economic benefit and reliability, Wind Eng. 24 (4) (2000), https://doi.org/10.1260/0309524001495639.
[42] P. Nguyen, A. Thorstensen, S. Sorooshian, K. Hsu, A. AghaKouchak, B. Sanders, M. Smith, A high resolution coupled hydrologic–hydraulic model (HiResFlood-UCI) for flash flood modeling, J. Hydrol. 541 (2016) 401–420, https://doi.org/10.1016/j.jhydrol.2015.10.047.
[43] M. Schneider, P. Priesmeier, A. Fekete, D. Lichte, F. Fiedrich, Cascading effects of critical infrastructures in a flood scenario: a case study in the City of Cologne, in: Proceedings of the International ISCRAM Conference, 2024, https://doi.org/10.59297/ws32ka31.
[44] B.D. Hoen, J.E. Diffendorfer, J.T. Rand, L.A. Kramer, C.P. Garrity, H.E. Hunt, United States wind turbine database v7.0 (May 10, 2024). U.S. Geological Survey, American Clean Power Association, and Lawrence Berkeley National Laboratory Data Release, 2018, https://doi.org/10.5066/F7TX3DN0.
[45] Iowa Department of Natural Resources, Iowa 30-meter digital elevation model (DEM). www.iowadnr.gov, 2022.
[46] Iowa State University Geographic Information Systems Support and Research Facility, GIS data: iowa soil drainage class maps (gSSURGO). www.agron.iastate.edu/glsi/gis-data/, 2021.
[47] C. Draxl, B.M. Hodge, A. Clifton, J. McCaa, Overview and Meteorological Validation of the Wind Integration National Dataset Toolkit (Technical Report, NREL/TP-5000-61740), National Renewable Energy Laboratory, Golden, CO, 2015.
[48] J. King, A. Clifton, B.M. Hodge, Validation of Power Output for the WIND Toolkit, National Renewable Energy Laboratory, Golden, CO, 2014. Technical Report, NREL/TP-5D00-61714).
[49] W. Lieberman-Cribbin, C. Draxl, A. Clifton, Guide to Using the WIND Toolkit Validation Code, National Renewable Energy Laboratory, Golden, CO, 2014. Technical Report, NREL/TP-5000-62595).
[50] C. Draxl, B.M. Hodge, A. Clifton, J. McCaa, The wind integration national dataset (WIND) toolkit, Appl. Energy 151 (2015) 355366.
[51] OpenStreetMap contributors, OpenStreetMap [Map], www.openstreetmap.org, 2015.
[52] W.R. Halter, Flood safety on dikes with wind turbines, in: Geotechnical Safety and Risk V, IOS Press, 2015, pp. 516–521, https://doi.org/10.3233/978-1-61499-580-7-516.
[53] C. Lavanya, N.D. Kumar, Foundation types for land and offshore sustainable wind energy turbine towers, E3S Web Conf. 184 (2020) 01094, https://doi.org/10.1051/e3sconf/202018401094.
[54] GEO-SLOPE International Ltd. www.geo-slope.com.
[55] Shweta Shrestha, Design and analysis of foundation for onshore tall wind turbines, All Theses. 2291. open.clemson.edu (2015).
[56] A.M.M. Pozo, P. Priesmeier, A. Fekete, Measuring spatial accessibility to critical infrastructure: the access road identification model, Int. J. Crit. Infrastruct. prot. 49 (2025) 100760, https://doi.org/10.1016/j.ijcip.2025.100760.

[57] L. Fang, X. Ding, T. Li, Analysis of optimal buffer distance for linear hazard factors in landslide susceptibility mapping, Sustainability 15 (13) (2023) 10180, https://doi.org/10.3390/su151310180.

[58] S. Pervez, N. Choudhary, R. Ranjan, A. Ahmad, N. Lodhi, Development of land-use regression model for seasonal variation of nitrogen dioxide ($NO_2$) in Lahore, Pakistan, Sustainability 13 (9) (2021) 4933, https://doi.org/10.3390/su13094933.

[59] Soil Science Division Staff, Soil survey manual, US Dep. Agric. Nat. Resour. Conserv. Service 18 (2) (2017). www.nrcs.usda.gov.

[60] S.S. Islam, S. Yeşilköy, Ö. Baydaroğlu, E. Yıldırım, I. Demir, State-level multidimensional agricultural drought susceptibility and risk assessment for agriculturally prominent areas, Int. J. River Basin Manag. (2024) 1–18, https://doi.org/10.1080/15715124.2024.2304546.

[61] D. Haynes, S. Manson, E. Shook, Terra Populus' architecture for integrated big geospatial services, Trans. GIS 21 (3) (2017) 546–559, https://doi.org/10.1111/tgis.12286.

[62] R. Saldanha, R. Akbarinia, M. Pedroso, V. Ribeiro, C. Cardoso, E.H. Pena, F. Porto, Zonal statistics datasets of climate indicators for Brazilian municipalities, Envrion. Data Sci. 3 (2024) e2, https://doi.org/10.1017/eds.2024.3.

[63] H. de Moel, B. Jongman, H. Kreibich, B. Merz, E. Penning-Rowsell, P.J. Ward, Flood risk assessments at different spatial scales, Mitig. Adapt. Strategies Glob. Change 20 (6) (2015) 865–890, https://doi.org/10.1007/s11027-015-9654-z.

[64] A. Narayanan, H.H. Willis, J.R. Fischbach, D. Warren, E. Molina-Perez, C. Story, K. Loa, L. Kendrick, P. Sorensen, T. LaTourrette, Characterizing National Exposures to Infrastructure from Natural Disasters: Data and Methods Documentation (RR-1453/1-DHS), RAND Corporation, Santa Monica, CA, 2016, https://doi.org/10.7249/RR1453.1.

[65] B. Tellman, U. Lall, A.K.M.S. Islam, M.A. Bhuyan, Regional index insurance using satellite-based fractional flooded area, Earths Future 10 (3) (2022), https://doi.org/10.1029/2021EF002418.

[66] P. Asaridis, D. Molinari, A conceptual model for the estimation of flood damage to power grids, Adv. Geosci. 61 (2023) 1–21, https://doi.org/10.5194/adgeo-61-1-2023.

[67] U. Kuckartz, S. Rädiker, T. Ebert, J. Schehl, U. Kuckartz, S. Rädiker, J. Schehl, Korrelation: zusammenhänge identifizieren, Statistik: Eine verständliche Einführung (2013) 207–237, https://doi.org/10.1007/978-3-531-19890-3.

[68] Ronald A. Fisher, Frequency distribution of the values of the correlation coefficient in samples from an indefinitely large population, Biometrika 10 (4) (1915) 507–521, stat.duke.edu.

[69] Federal Emergency Management Agency, FEMA Policy 206-24-005: Federal Flood Risk Management Standard (FFRMS), U.S. Department of Homeland Security, 2024. www.fema.gov.

[70] A. Mondal, P.P. Mujumdar, Detection of change in flood return levels under global warming, J. Hydrol. Eng. 21 (8) (2016) 04016021, https://doi.org/10.1061/(ASCE)HE.1943-5584.0001326.

[71] L. Lledó, O. Bellprat, F.J. Doblas-Reyes, A. Soret, Seasonal forecasts of wind power generation, Renew. Energy 143 (2019) 91–100, https://doi.org/10.1016/j.renene.2019.04.135.

[72] Pacific Northwest National Laboratory (PNNL), Distributed Wind Guidebook (PNNL-36577), U.S. Department of Energy, Richland, WA, 2025. www.pnnl.gov.

[73] U.S. Department of Energy (DOE) WINDExchange, A breezy guide to help you navigate WINDExchange, 2023, January 30.

[74] International Electrotechnical Commission (IEC), IEC 61400-1: Wind Energy Generation Systems — Part 1: Design Requirements, fourth ed., 2019. Geneva, Switzerland: IEC.

[75] J.F. Manwell, J.G. McGowan, A.L. Rogers, Wind Energy Explained: Theory, Design and Application, second ed., Wiley, 2010 https://doi.org/10.1002/9781119994367.

[76] T. Lewin, An Investigation of Design Alternatives for 328-ft (100-m) Tall Wind Turbine Towers, Iowa State University, 2010, https://doi.org/10.31274/etd-180810-2978.